ELECTRO-THERMAL BREAKDOWN OF HVDC CABLES AND EFFECT OF LONG-TERM AGEING ON SPACE CHARGE IN CABLE DIELECTRICS

PhD Thesis

by

SATHYAMOORTHY DHAYALAN

DEPARTMENT OF ELECTRICAL ENGINEERING
INDIAN INSTITUTE OF TECHNOLOGY ROPAR
RUPNAGAR-140001 (INDIA)

June, 2023

ELECTRO-THERMAL BREAKDOWN OF HVDC CABLES AND EFFECT OF LONG-TERM AGEING ON SPACE CHARGE IN CABLE DIELECTRICS

A Thesis Submitted

In Partial Fulfilment of the Requirements

For the Degree of

DOCTOR OF PHILOSOPHY

by

SATHYAMOORTHY DHAYALAN

to the

DEPARTMENT OF ELECTRICAL ENGINEERING

INDIAN INSTITUTE OF TECHNOLOGY ROPAR

RUPNAGAR-140001 (INDIA)

June, 2023

“Dedicated to my great father, Dhayalan. N, who always believed that education can transform a person. You are no more, but the wisdom you have imparted to us shall remain in our hearts forever. “

INDIAN INSTITUTE OF TECHNOLOGY ROPAR
PUNJAB, INDIA

CANDIDATE's DECLARATION

I hereby certify that the work which is being presented in the thesis, entitled "**Electro-Thermal Breakdown of HVDC Cables and Effect of Long-Term Ageing on Space Charge In Cable Dielectrics**" in partial fulfilment of the requirements for the award of the Degree of Doctor of Philosophy and submitted to the Department of Electrical Engineering of the Institute is an authentic record of my own work carried out during a period from January 2017 to June 2023 under the supervision of Prof. Ch. Chakradhar Reddy.

The matter presented in this thesis has not been submitted by me for the award of any other degree of this or any other University/Institute.

(Sathyamoorthy **Dhayalan**)
(2016EEZ0016)
Signature of the candidate

This is to certify that the above statement made by the candidate is correct to the best of my knowledge.

Date: 25/09/2023

(Prof. Ch. Chakradhar Reddy)

Professor
Department of Electrical Engineering
Indian Institute of Technology Ropar

The Ph.D. Viva-Voce examination of Sathyamoorthy Dhayalan, Research Scholar, has been held on: 26 June 2023.

ABSTRACT

With the advent of High Voltage Direct Current (HVDC) technology, underground power cable transmission, with polymeric insulation, owing to its several inherent benefits, is eclipsing over the conventional mass impregnated and oil-impregnated paper insulation. Polymeric HVDC cables have excellent electrical and thermal properties, especially in design stress, which is comparatively high, compared to mass and oil-impregnated insulation. In general, cable performance has assumed paramount importance in power transmission. The performance of power cables is linked to the electric and thermal profiles of the dielectric. Standard recommendations, such as CIGRÉ TB-496 and IEC-62067, provide guidelines for manufacturers as well as utilities for the testing of cables. However, for high voltages (more than ~500 kV) extruded cable technology is still limited mostly to laboratory or developmental experience. Therefore, it is important to have viable simulation tools, not only for design and development but also for the condition assessment of the cables. This work presents the simultaneous simulation of interdependent electric and thermal fields inside a dc cable, under loaded conditions using analogous distributed circuit models for thermal and electrical phenomena. The complex nonlinearities are integrated with such circuit models, leading to the simulation of electro-thermal runaway, for the first time, in a dc cable. Using the suggested, nonlinear circuit models, complete dynamics of the temperature profile and electric field inside the cable dielectric can also be obtained under various test and operating conditions until electro-thermal runaway limits in the time domain. The results are useful for the design and development of dc cables with safety factors, apart from understanding the electro-thermal limits. The models are validated with rigorous and careful experiments.

In general, when the polymeric cable operates under continuous load and sometimes under overloaded conditions, it is subjected to high thermal stress, which causes polymer degradation. Ageing is a slow process, causing the weakening of insulation. In HVDC cables, space charge accumulation inside the bulk of cable insulation is a major issue which has been deemed critical to their breakdown and thus is a topic of great interest in the HVDC cable industry. However, space charge is not that severe issue in the case of High Voltage Alternative Current (HVAC) cables due to

periodic polarity changes. Space charge is known to accumulate even in a fresh specimen, however, particularly in an aged polymeric material, due to the degradation of the material, space charge is believed to be extremely significant. The presence of space charge in the insulation bulk affects the electric field, making its distribution non-uniform across the insulation, which may cause a premature breakdown in the insulation. So, in this work, the author intends to investigate the effect of long-term thermal ageing on the accumulation of space charge and electric field dynamics in a polymeric material (LDPE-Low-Density Polyethene), which is a widely used base material for polymeric cable insulation). To achieve thermal ageing, the prepared LDPE sheet samples were placed in a hot air oven for long durations. Thermal ageing has been carried out under different ageing temperatures and durations. The space charge was measured after certain ageing periods using the PEA (Pulsed Electro-Acoustic) method. The experiments were done for low and high electric fields. All experiments were done at ambient temperature. The corresponding electric field enhancement has been investigated. The space charge density and electric field enhancement factors have been estimated. Also, in highly aged samples (256 days), the space charge is measured in the vicinity of breakdown. A clear difference in the trend of packet-like charge movement is observed in the highly aged samples when compared to the packet charge of fresh samples reported until now. Interesting insights on the injection and movement of charges through the bulk, mean accumulated charge density, field enhancement factor, as well as the shift of space charge regimes with ageing, are presented, which were apparently not given adequate attention in the literature so far. The results are believed to be useful for HVDC insulation designers and utilities.

ACKNOWLEDGEMENT

First of all, I thank the almighty for allowing me to walk on this path. It has been an unforgettable journey full of exploration and self-discovery.

I extend sincere thanks and gratitude to my supervisor Prof. C. C. Reddy, Professor, Department of Electrical Engineering for giving me the opportunity to work with him and persevering with me in difficult times. He has been a constant source of guidance and pragmatic advice in this journey.

I am thankful to Prof. Rajeev Ahuja, Director, IIT Ropar, and Prof. S. K. Das (Ex-Director, IIT Ropar) for their constant support. I also thank Dr. S. Murala, Head of Department (Electrical Engineering) for providing the required facilities for my research work. I also thank my doctoral committee members: Prof. J. S. Sahambi, Dr. S. Murala, Dr. J. Kalaiselvi, and Dr. G. Sankara Raju.

My acknowledgments are also due to Mr. Dilbag Singh (EED) and Mr. Jaspreet Singh (EED) for their help in the experimental works and encouragement. I am indebted to the many hard-working individuals at the Department of Electric Engineering. The administration at our department often does work behind the scenes, but its efforts are immensely important to us.

I appreciate the help given by my senior colleagues Dr. Jaspreet Chahal Singh, Dr. Alampratap Singh Tiwana, Dr. Ashish Gupta, Dr. Avnish Kumar Upadhyay, my friends especially Dr. Ajith John Thomas, Dr. Birender T. Singh, Iyyapan, Purnabhishek, Pranav Johri, Aritra, Bibhav, Harshith, Priyesh, Venky, Aayushi, Nithin, Parimal, Manika, Bura Rajesh, Pankaj, Jaswant, Sathish, for being ever prepared to assist me and supporting me during the course of my study. A special thanks to all.

It is only through the support of my mother, family and friends that this work is possible. Special thanks to my sister and uncle for their valuable support. No words can express my wife’s unconditional support during critical time. She has been a pillar of my strength during the course of this entire journey. A special thanks to my lovely children.

Finally, I would like to thank Prof. N. Gupta (IIT Kanpur), Prof. U. Kumar and Prof. L. Satish (IISc Bangalore) and Prof. L. A. Dissado (University of Leicester), Toshikatsu Tanaka and Yoshimichi Ohki (Waseda University) for their valuable suggestions and encouragement, during their visit to the Dielectric Measurements Lab at IIT Ropar.

Indian Institute of Technology Ropar (Sathyamoorthy Dhayalan)

Date: 26-06-2023

Contents

List of tables

List of symbols

E	Electric Field *(kV/mm)*
V	Voltage *(kV)*
k	Thermal conductivity at $293\ K$ $(W/(m.K))$
α	Coefficient of thermal conductivity in $(W/(m.K^2))$
r	Thermal resistance (K/W)
c	Thermal capacitance (J/K)
s	Specific heat capacity in $(J/(kg.K))$
ρ	Mass density (kg/m^3)
i	Thermal current source (W)
R	Electrical resistance (Ω)
C	Electrical capacitance (F)
I	Electrical current (A)
σ	Insulation conductivity (S/m)
A	Conductivity coefficient of insulation (S/m)
a	Stress coefficient (m/V)
b	Temperature coefficient (K)
ε_0	Vacuum permittivity *(F/m)*
ε_r	Relative permittivity
T	Temperature *(K)*
ΔT	Temperature difference *(K)*
Q	Space charge density (C/m^3)

List of figures

Abbreviations

Abbreviation	Description
HDPE	High Density Polyethylene
HVAC	High Voltage Alternating Current
HVDC	High Voltage Direct Current
PE	Polyethylene
LDPE	Low Density Polyethylene
PEA	Pulsed Electroacoustic
PVDF	Polyvinylidene Fluoride
XLPE	Cross Linked Density Polyethylene
BDV	Breakdown Voltage
LS	Least Squares
PVC	Poly Vinyl Chloride
LCC	Line Commutated Convertor
OIP	Oil-Impregnated Paper
FEF	Field Enhancement Factor
MIND	Mass impregnated paper
MTV	Maximum Thermal Voltage
FEM	Finite Element Method

CHAPTER 1

Introduction

1.1 Background and Motivation

With the development of power electronics devices in the 21st century, there is widespread use of High Voltage Direct Current (HVDC) because of their several advantages over High Voltage Alternating Current (HVAC) systems. For transferring bulk power over long-distance HVDC is a better choice compared to HVAC system. HVDC power transmission does not have the problem of reactive power compensation. Also, the DC converter station is used to interconnect to synchronise two different frequency systems. Even though the establishment of HVDC converter station is costlier, HVDC is cheaper when compared with the HVAC system for overhead transmission [1], for transferring the same amount of power over a long distance (>600 Km). High voltage cables are now preferred over overhead lines worldwide to transmit electric power. HVDC cables have certain advantages over HVAC cables, such as no continuous charging and discharging currents, non-requirement of reactive power compensation, no limitation in the power transmission length, etc. HVDC cables are cost-effective over more than 50 km (approx.) compared to HVAC [2-4]. The comparison of HVDC and HVAC cable cost versus power transmission distance is shown in Fig. 1.1 (a)

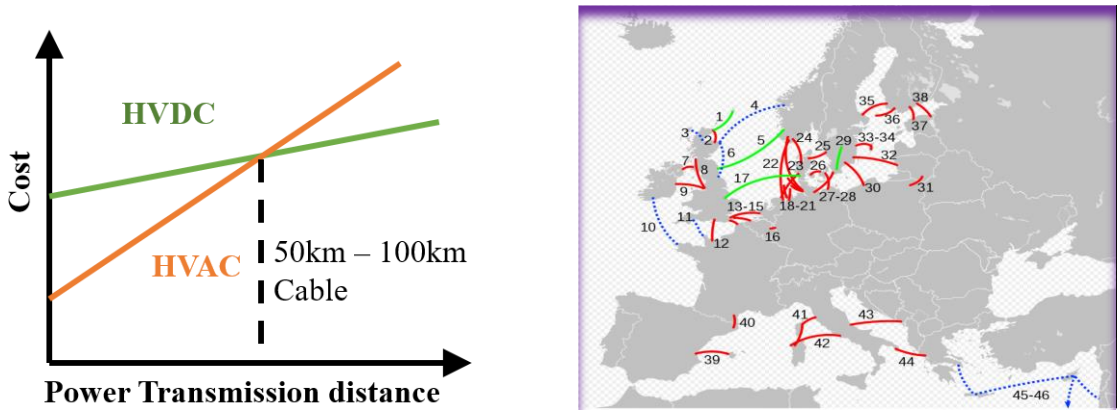

Fig. 1.1 (a) Comparison of HVAC and HVDC cable (b) Major HVDC lines in Europe. (https://en.wikipedia.org/wiki/High-voltage_direct_current)

HVDC cables are a viable option in special cases, such as geographical barriers, island power interconnections, the crossing of long rivers, lakes, etc. They are also a feasible option for connecting renewable energy sources such as solar and tidal power placed over long distances, with the grid. The major HVDC lines in Europe are shown in Fig 1.1 (b). The essential component to withstand such high voltage in a power cable is the insulation. Polymeric insulation is most commonly used for high voltage applications due to several advantages, like being maintenance-free, high resistivity, high breakdown strength, lower losses, good water resistance and high operating temperature, compared to oil-impregnated paper (OIP). Due its long-term benefits, especially on design stress and other advantages, it has replaced the mass impregnated (MIND) paper insulation, at almost all voltage levels [5]. The structure of a typical polymeric HVDC cable is shown in Figs 1.2 and 1.3.

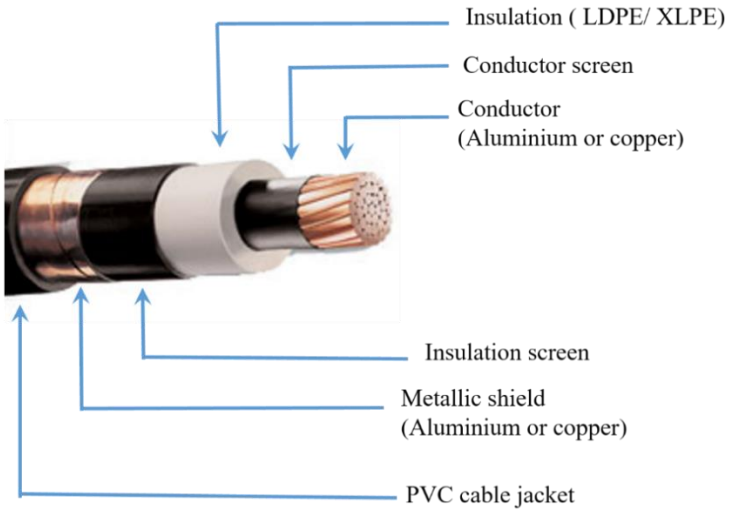

(www.nassaunationalcable.com)

Fig 1.2. Typical HVDC Polymeric power cable Construction

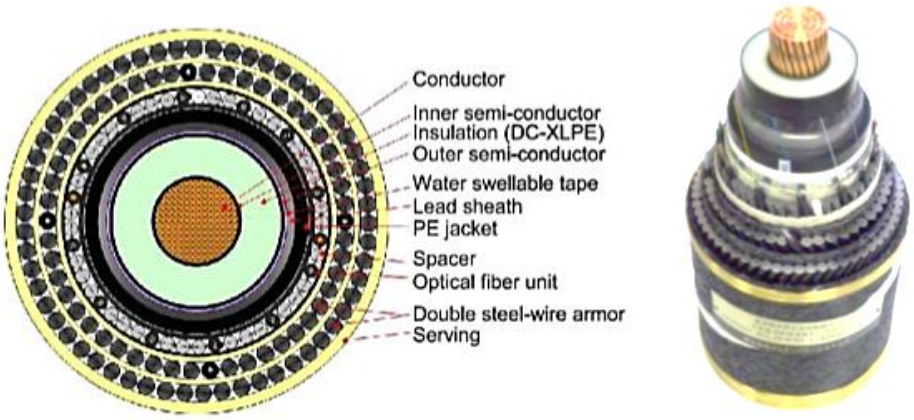

(a) (b)

Fig 1.3. A HVDC XLPE submarine cable (±250 kV) (a) Top view, (b) Side view [6], [7].

Power demand has been increasing day by day. As a result of this, we are going for higher voltage for bulk power transmission. The laying length of cables is also increasing day by day as shown in Fig 1.4.

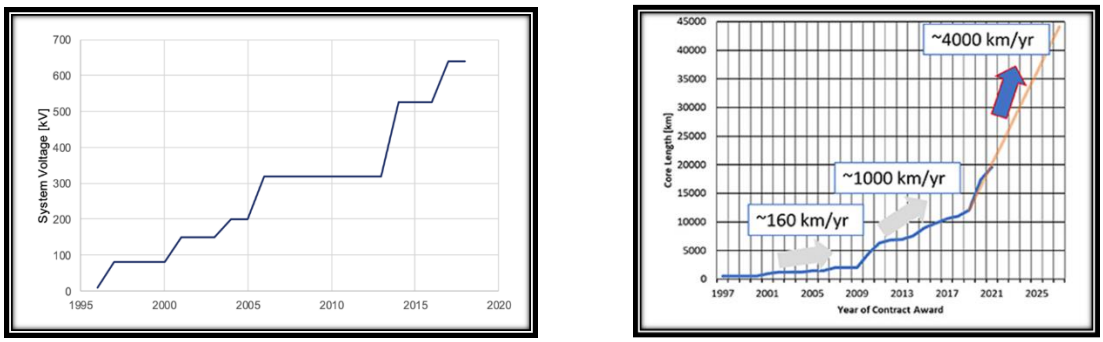

(a) (b)

Fig 1.4. (a) The trend of system voltage and (b) laying cable length per year. (https://www.inmr.com/quality-assurance-quality-control-of-hvdc-cable-systems/)

1.1.1 Electro-Thermal Breakdown in HVDC Cables

As is well known, insulation is the most important aspect of any high voltage equipment or system. Once insulation breakdown occurs, the entire electrical system may get collapsed. So, it is necessary to understand the behaviour and characteristics of insulation under different stress conditions. Several research papers explained about insulation failure that occurs due to either electrical or thermal stress [8], [9]. But in actual practice, the high voltage cable is subjected to both electrical and thermal stress simultaneously. Breakdown occurs mainly due to weakest point in the insulation. The underlying phenomenon of breakdown is believed to be filamentary and gets initiated in form of a local thermal breakdown at the weak point.

Once laid, power cables are expected to run satisfactorily for 30-40 years. In the long term, the insulation undergoes high electro-thermal stress, and this stress rises whenever a transient happens, especially during polarity reversal.

The standards for testing extruded cable systems under different test conditions are available for only up to certain voltage levels, above which research and development is still under process [10]. When cable is operating under bipolar transmission (LCC- Line Commutated Converter), voltage polarity reversal is done to change the power flow direction. During polarity reversal, the cable insulation is subject to high Laplacian field [11], [12]. With the increase in switching frequency (i.e. shorter duration of reversal), the insulation material may degrade rapidly, which may ultimately result in premature failure.

A theoretical formulation for computation of electric field and temperature distribution across HVDC cable under steady state, the maximum permissible temperature in insulation and thermal instability of cable was reported in [13].

One of the main contributions of the present work is the simulation of electro-thermal runaway in time domain. An inter-dependent electro-thermal circuit model is formulated, which may make it convenient to model the complete dynamics of the temperature profile and electric field inside the cable dielectric under various test and operating conditions until electro thermal runaway limits in time domain. The simulation model also incorporates the effect of external factors such as load current, ambient temperature and the surrounding medium (surrounding the cable e.g. soil).

Another significant contributions of this thesis is the development of an experimental setup for determining breakdown strength of a loaded HVDC cable under various load currents and environmental conditions. A special HV electrode has been developed which is capable of avoiding 'edge breakdown', which is a frequently encountered problem in cable breakdown tests. The simulation results were validated by comparison with experimental results.

1.1.2 Accumulation of Space Charge in polymeric Insulation under HVDC Fields

The second part of this thesis relates to the space charge in Low-Density Polyethylene (LDPE), which is the base polymer for all polymeric cables. When a dielectric material is subjected to an electric field, dipoles are aligned in the direction of the applied field. The charges within the dipoles are bound charges and other than the dipoles, a dielectric is not expected to have any other charge within its bulk. Thus, in an ideal dielectric, no space charge formation occurs and a uniform electric field distribution occurs across the insulation. The dipole formation and the electric field distribution across insulation are shown in Figs 1.5. (a) and (b) respectively [14].

In any practical dielectric, however, charges are formed within the bulk, which is primarily due to charge injection from electrodes; the presence of impurity or cross-linking agents such as in cross-linked polyethylene (XLPE) may also be responsible for these charges [15], [16]. Since these charges occur within the space of a dielectric, they are referred to as space charges. If the polarity of a space charge in the vicinity of the electrodes is same as the polarity of electrode, it is called homo charge.

Because of this non-uniform electric field occurs across the insulation. The field enhancement occurs in the middle of the bulk material. The homo charge formation and corresponding electric field distribution across insulation are shown in Figs. 1.5 (c) and (d) respectively. Over time, charges may slowly move from one electrode to another. Thus, when opposite polarity charges are present near the electrode, they are called hetero charges. In the case of hetero space charge, the field enhancement occurs at both ends of the insulation [17]. The formation of hetero charge in the insulation and corresponding electric field distribution across the insulation are shown in Figs. 1.5 (e) and (f) respectively. The presence of either homo or hetero space charge, thus leads to field enhancement in the insulation, so that the maximum field is above the value of the design electric field. Due to this, a particular portion of the insulation continuously encounters higher stress. Due to this, over long periods, the insulation gets deteriorated at a rate much faster than usual and this may cause premature breakdown [18-20].

In this work, the author aims to investigate the effect of long-term thermal ageing on the space charge characteristics of LDPE. To this end, LDPE sheet samples were prepared and thermally aged systematically in batches, at different temperatures and for different time durations. Space charge was measured for a large number of samples from each thermally aged batch and inferences were drawn based on parameters such as charge density, field enhancement factor (FEF) and net charge density, among others. In case of highly aged samples, space charge was measured until breakdown and a possible mechanism relating the DC dielectric breakdown with space charge accumulation is presented.

(Normal polarization)

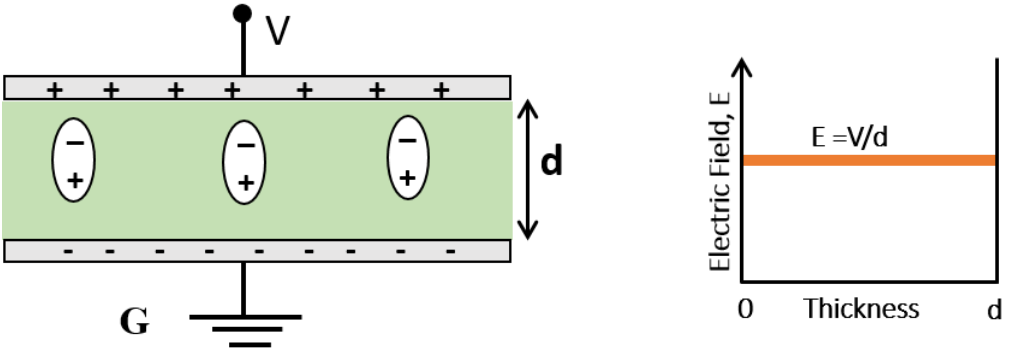

(a) (b)

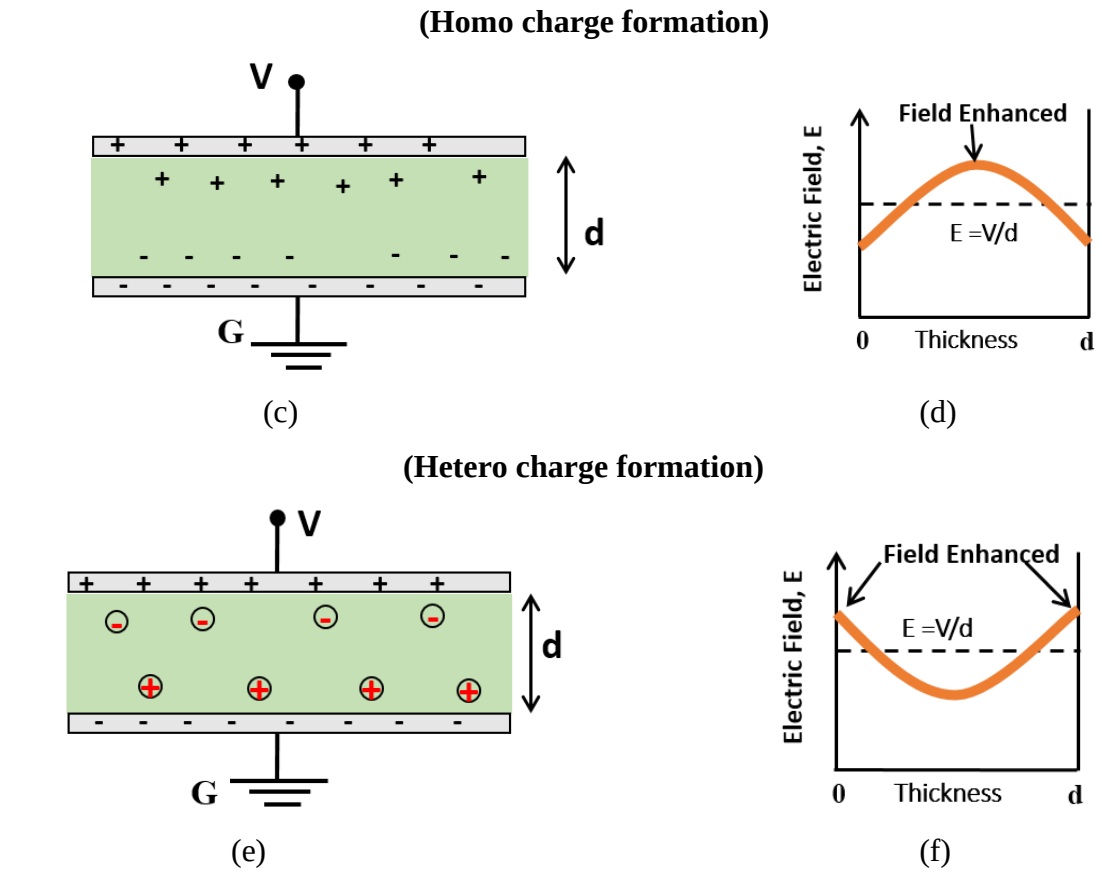

Fig. 1.5. (a) Polarization of dielectric under ideal case, (c) Homo space charge formation, (e) Hetero space charge formation, corresponding electric field across insulation is (b),(d) and (f).

1.2 Thesis Organization

The thesis is organized in 5 chapters. A brief description of each chapter is given below:

Chapter 1 Introduction

This chapter presents a general introduction to the HVDC cables, their advantages over HVAC cables and significance of polymeric insulation. The two main parts of this thesis are then briefly described which are: electro-thermal breakdown in cable insulation and space charge accumulation respectively. The main contributions of this thesis are highlighted and their significance in context of HVDC cables is discussed.

Chapter 2 Literature Review - Problem Definition

This chapter presents a comprehensive review of the existing literature. The research gaps in many of the existing models for electro-thermal modelling are described, which include the assumption of constant conductivity, neglecting dielectric losses in the electro-thermal model, among others. Also, a review is given of existing literature on

space charge in LDPE and its implications on the failure of cable insulation. Finally, the research problem is formulated.

Chapter 3 Simulation and Experiments on the Electro-Thermal Breakdown of HVDC cable

In this chapter, the developed distributed electro-thermal circuit model of a HVDC cable has been presented along with the various experimental setups. The circuit (simulation) model considers all the layers of a typical submarine cable and the experimentally measured cable conductivity is incorporated in the electrical circuit model. Also, the losses in the various layers act as heat sources in the thermal circuit. The simulations were then carried out for different operating conditions such as the load cycle as per the Cigré TB 496 standard. Also, both transient and steady-state behaviour of cable has also been simulated and temperature and electric field in the insulation were estimated. The cable was simulated up to breakdown and the effect of load, ambient temperature and soil on the breakdown is investigated. The different between intrinsic and interactive instability has been shown. Then, the developed experimental setup for breakdown test of loaded HVDC cable is described along with the three-electrode setup for measurement of volumetric leakage current to estimate DC conductivity. The various simulation and experimental results are presented and inferences are drawn.

Chapter 4 Thermal Ageing and space charge measurement accumulation in aged LDPE under HVDC

This chapter presents the thermal ageing of LDPE and its effect on the space charge accumulation in detail. The methodology of sample preparation is presented and the setup used for long-term thermal ageing is described. Also, the pulse electro-acoustic (PEA) setup, which has been used to measure the space charge in fresh and aged samples, in this work is described. The profile and dynamics of space charge (i.e. homo charge, hetero charge, packet charge) for each batch of thermally aged samples is presented. Also, the corresponding electric fields, FEF and net charge are estimated. The space charge characteristics until breakdown are presented for highly aged samples and an associated mechanism, relating these two phenomena is described.

Chapter 5 Conclusions and Future Scope of the Work

In this chapter, the tangible conclusions of this thesis are summarized along with the future scope of this work.

CHAPTER 2

Literature Review- Problem Definition

2.1. Literature Survey on Electro-Thermal Modelling and Breakdown of Cable Insulation

With an increase in the use of HVDC technology around the world for grid interconnections and tapping of power from alternate sources of energy, cable performance has assumed paramount importance. The performance of power cables is linked to the electric and thermal profiles of the dielectric. Standard recommendations such as CIGRÉ TB-496 [21] and IEC-62067 [22], provide guidelines for manufacturers as well as utilities for the testing of cables. However, for high voltages (more than ~500 kV) extruded cable technology is still limited mostly to laboratory or developmental experience [21]. Therefore, it is important to have viable simulation tools, not only for design and development, but also for the assessment of the cables.

The role of multi-factor dependent electrical conductivity on steady-state temperature and electric fields in dc cables is well known [23], [24]. Theoretical maximum limits on power handling capacity of HVDC cables and estimation of thermal maximum voltages for cables have been formulated, based on temperature limitations of the insulation [25] under steady-state limiting conditions. The thermal breakdown phenomenon has received considerable focus [26], [27] due to the dynamic interdependence of electric and thermal fields under dc. Furthermore, the mode of failure of extruded cables is believed to be thermal [28]. The punctured polymeric cables is shown Fig 2.1. It is important to see thermal runaway and limiting conditions, in time domain, to better understand, evaluate and design power cables. As per the literature based on finite element method (FEM), on transient behavior of HVDC cable, simulation of electric field and temperature has been reported in [29], however, joule losses in insulation were neglected. Ignoring such losses may not affect the electric field and temperature computations for voltages less than the breakdown level, however, it has a significant effect at high fields, where, a positive feedback would occur between the fields due to field-temperature aided conduction in dielectrics [23].

(a)

(b)

(c)

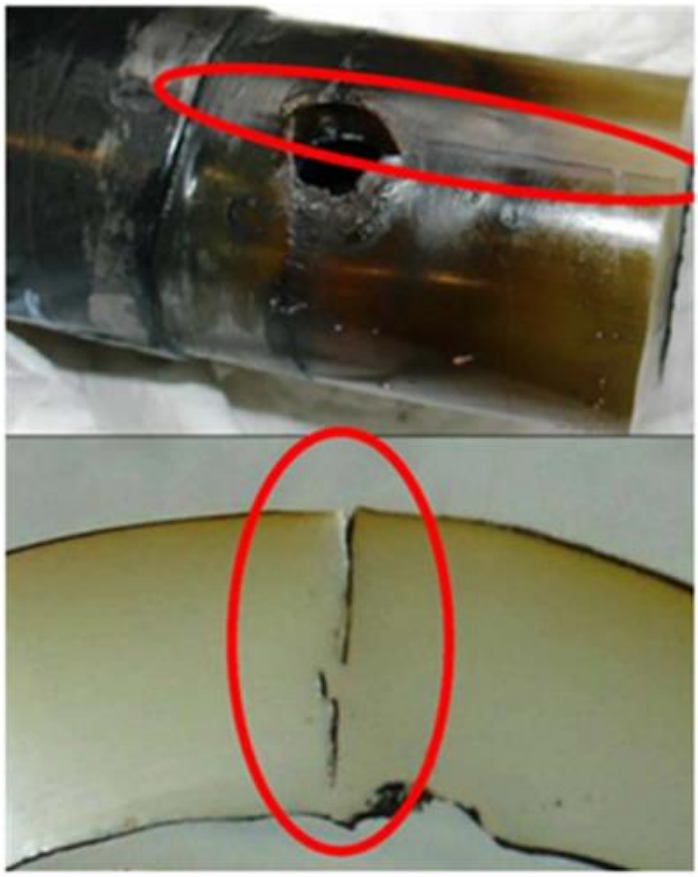

(d)

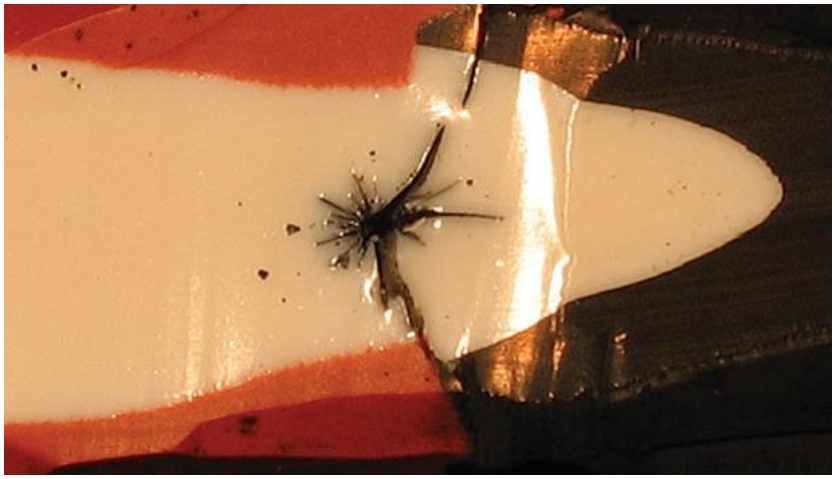

(e)

Fig: 2.1 (a) Punctured cable received from Adani Electricity, Mumbai. India (Under Investigation). (b) & (c) Completely burnt cables after breakdown due to high temperature. (d) & (e) internal view of punctured cables (courtesy: https://www.assemblymag.com/, https://www.powerandcables.com/, ttps://ietresearch.onlinelibrary,wiley.com/)

In Another paper [30] based on FEM, enhancement of electric field in a cable termination (2-D model) is reported, where, constant conductivity was considered in the model, which, again, cannot produce the cascading positive feedback effect at high fields. Numerical techniques for evaluation of losses, heating and ampacity for buried AC cable systems were also reported in [31], [32] without reference to electric field, but with a focus on ampacity, while, the thermal runaway was not considered. Further, it was reported that there are difficulties of convergence near breakdown in numerical simulations.

As per the literature related to the use of circuits for modelling thermal behavior, a lumped circuit model, where, insulation was modeled as one unit, to find out ampacity for AC cable system is reported in [33], [34]. However, thermal capacitance was not incorporated in the thermal circuit in [33], which cannot simulate a transient behavior, although the insulation losses (constant ac conductivity) were represented using lumped circuit parameters. In [34], only conductor losses were considered in a lumped circuit, whereas insulation ohmic loss was neglected. These models being lumped circuit models, electric field, temperature distribution and thermal runaway cannot be obtained.

While [33] and [34] report for AC cables, in another work based on circuit models [35], time domain electric field and temperature in medium voltage dc cables (used in a ship) has been reported. However, only the losses due to conductor were considered, while heat generated due to insulation losses was not incorporated, which is shown in this work to have an important role on thermal runaway.

However, the transient electro-thermal runaway in a dc cable is believed to have not been reported until now. For example, the thermal and electrical circuits have different time constants and also have inter-dependency. A loaded cable will undergo dynamic change in electric field with load variations and switching. Therefore, it is considered important to investigate the dynamic electro-thermal behavior of an HVDC cable under different conditions.

2.2. Literature Survey on Accumulation of Space Charge in Polymeric Insulation

Space charge accumulation [40], [41] under HVDC fields is a widely reported problem in polymeric insulation. It is known that space charge distorts the local electric field, which may lead to field enhancement and thereby affect the dielectric strength [42]. Polymeric insulation is used in various HVDC applications, such as power cables, where the insulation is stressed both electrically and thermally [43]. Under prolonged thermal stress, irreversible physical and chemical changes may occur [44], which may deteriorate the insulation, eventually leading to premature breakdown. The space charge dynamics in fresh LDPE samples are based on history of long time applied voltage and the polarity of charge formation is dependent on applied voltage [45].

Space charge in LDPE at pre-breakdown was reported in [46], where fresh LDPE samples were subjected to increasing fields up to 300 kV/mm and then kept constant until breakdown. Space charges were recorded for a short duration of 300 ms at different temperatures. High amount of positive charge injection was found to be major contributing factor in intrinsic breakdown of fresh LDPE. The space charge in fresh LDPE samples was further investigated at different fields until breakdown in [47], [48]. Space charge profiles until breakdown in fresh LDPE is shown in Fig 2.2. These results further confirmed the existence of large positive packet charges which were injected at anode and stopped at certain position near the cathode, which was followed by breakdown. However the space charge dynamics until breakdown were investigated for only fresh LDPE samples. In [49],[50], it was shown that addition of nanocomposites in fresh LDPE suppressed space charge formation, and resulted in the improvement of breakdown strength for the fresh LDPE samples. The space charge was experimentally measured at 30 kV/mm for individual sections of a HVDC cable [51], which were thermally aged for up to 1000 hours at 106 ℃. In another work [52], LDPE samples were thermally aged for a short duration of 360 hours at 90℃. Space charge measurements were performed at -50 kV/mm, and were compared with other insulation materials of polyethylene family, viz., HDPE (High-Density polyethylene), FPE (Foamed polyethylene). However, Space charge dynamics in polyethylene materials for short-term ageing has been reported.

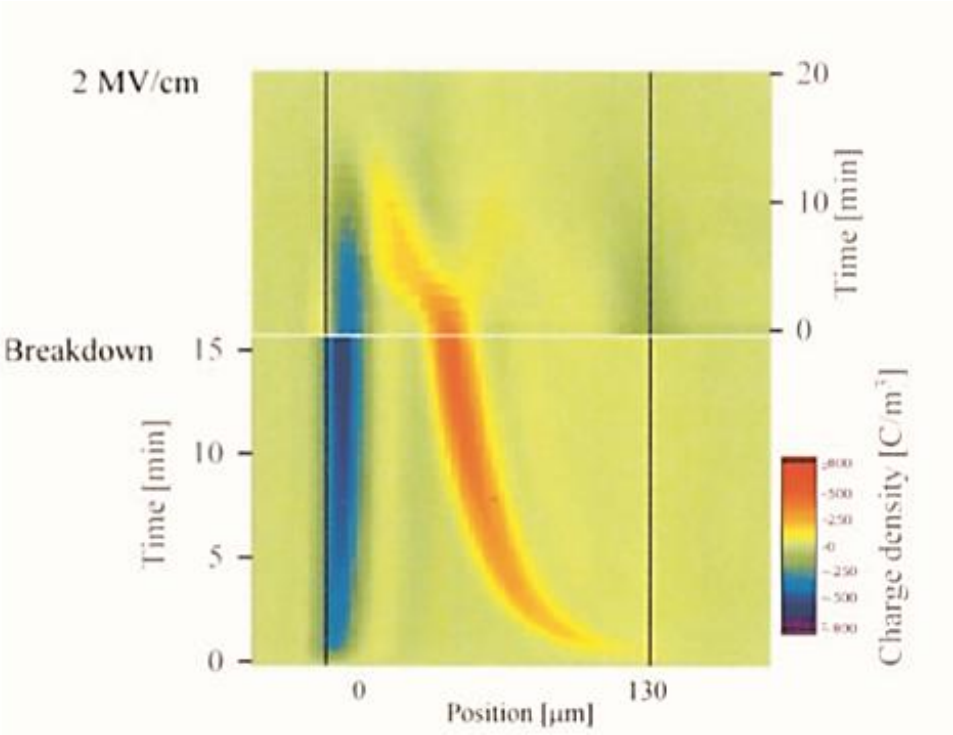

Fig 2.2. Space charge profiles until breakdown in fresh LDPE (thickness of 130 μm) under applied electric field 2MV/cm [47].

Thermal endurance stress tests have been done for 160 kV HVDC cable insulation , as reported in [53] and the effect of thermal ageing on crystallinity, space charge and other physicochemical properties was presented. It was inferred in [53] that the change in insulation properties will affect the space charge formation. However, space charge measurements were done only under low electric fields (up to 20 kV/mm).

It may be safely said that all three phenomena, viz. space charge accumulation, ageing and breakdown, are closely interrelated and hence, understanding the dynamics of space charge accumulation in polymeric material under long term thermal ageing and associated breakdown is of utmost importance.

A clear lacuna is observed in literature regarding space charge accumulation under long term thermal ageing. Investigation of space charge dynamics until breakdown for highly aged samples has not received adequate attention till now. Moreover, polymeric insulation is expected to operate between 70°C to 80°C in practical applications, at which the space charge characteristics might differ from that of accelerated ageing that were reported earlier [53].

Hence, in this work, the author attempts to investigate the space characteristics in thermally aged LDPE. The LDPE sheet samples are subjected to long-term thermal ageing (up to 256 days) at different temperatures, that are close to the actual operating temperatures and space charge measurements are performed under both low and high fields. Also, the net charge in the bulk and field enhancement factor were estimated. The space charge was also experimentally measured until and after breakdown for highly aged samples and a possible associated mechanism of breakdown has been investigated.

2.3 Overview of Literature

2.3.1 Problem Statement

Based on the literature review, the limitations of the electro-thermal model have been identified. Also, the dependence of space charge accumulation in cable insulation on ageing temperatures and duration has not been investigated extensively, particularly until breakdown. Based on the research gaps, the following objectives are thus proposed:

- To develop a comprehensive simulation model to simulate the complete electro-thermal dynamics until breakdown of a HVDC power cable, while incorporating
    - Experimentally measured non-linear DC conductivity of cable insulation
    - Effect of load current and ambient temperature
    - Effect of depth of cable and soil thermal properties.
- To develop a novel experimental setup for breakdown test of a loaded HVDC cable, under different load currents and environmental conditions, while avoiding the problem of edge breakdown.
- To experimentally investigate the space charge dynamics in thermally aged LDPE samples under both low and high fields.
- To understand the space charge dynamics until breakdown, also to estimate the net charge, electric field, FEF, anode and cathode charges until breakdown for long term aged samples.

2.3.2 Methodology used in achieving the objectives

To achieve the desired objectives of the first part of the thesis, it all started with a small circuit model for the simulation, then, after considering all the layers of HVDC cable, including soil, a comprehensive, distributed electro-thermal circuit model was developed (as described in detail in Chapter 3). The simulation model incorporates the experimentally measured conductivity. To validate the simulation model, an electro-thermal breakdown setup was developed for cable with an aim to rectify the problem of edge breakdown in cable.

The work for second part of this thesis began with the preparation of LDPE sheet samples from granules using a two-roll mill and hydraulic press. The prepared samples were kept in the oven at different temperatures and periods for thermal ageing. The space charge measurements were then conducted on thermally aged samples under low as well as high electric fields to investigate accumulation of space charge (as described in detail in Chapter 4). Also, the space charge profile was examined until the breakdown for highly aged samples.

CHAPTER 3

Simulation of Electro-thermal Runaway and Thermal Limits of a Loaded HVDC Cable

3.1 Introduction

The performance of power cables is directly linked to the electric and thermal profiles of the dielectric. It is known that the HVDC cables have no limit on the length, due to the absence of steady state capacitive reactive power, unlike the HVAC cables which are intensely fraught with reactive power. However, the strong dependence of insulation conductivity on electric stress and temperature puts constraints on the power handling limits of HVDC cables. Also, due to unavoidable circumstances, the cable may get subjected to high loads and sudden switching operations, during which high electro-thermal stress is experienced by the insulation, which leads to its faster degradation. The presence of such transients, thus also acts as a constraint to the power transfer capability of the cable. The presence of external thermal resistance due to soil surrounding the cable, changes the electro-thermal phenomena in the cable from being intrinsic to interactive breakdown. In view of the mentioned reasons, HVDC cables need to be operated within certain limits of voltage and load current to maintain their electro-thermal stability. The maximum thermal voltage (MTV) is defined as the maximum voltage upto which an HVDC cable under no-load stabilizes [25], but beyond which the instability is bound to occur, due to an internal cascading. However, the MTV reduces considerably when the cable operates under loaded condition. This chapter presents the simultaneous simulation of interdependent electric and thermal fields inside a dc cable under loaded conditions using analogous distributed circuit models for thermal and electrical phenomena, while incorporating the nonlinearities in such circuit models, leading to simulation of electro-thermal runaway, for the first time, in a dc cable. The experimental breakdown setup for loaded HVDC cable is also described and the results are presented and compared with the simulation results.

3.2 Electro-Thermal circuit model

As heat flow is analogous to current flow, voltage to temperature, thermal conductivity to electrical conductivity, thermal capacity to electrical capacitance, the thermal behavior of the cable layers and surroundings is modeled as a distributed parameter, 'analogous electric circuit', hereafter called as 'thermal circuit', while the name 'electric circuit' is reserved for electric behavior, as presented later.

Unlike previous works (AC circuits of [33], [34], and DC circuits of [35]), the interdependence between thermal circuit and electric circuit is accounted for in both the thermal and electric circuits. The current sources in the thermal circuit corresponding to heat produced are due electrical phenomenon (joule losses) and hence depend on electrical quantities of the electric circuit presented later. Also, the electrical circuit components do depend on temperature and hence on thermal circuit node voltages.

3.2.1 Modeling with Discrete Concentric Cylinders

Referring to Fig. 3.1 (a), a HVDC underground cable, with all its layers, has been modeled by dividing them into several concentric cylindrical strips/elements of small thickness (Fig. 3.1 (b)), each having respective thermal and electrical parameters, as mentioned in Table 3.1. A HVDC cable in operation and the heat flow direction from conductor to surrounding medium (through all layers) are shown in Figs 3.1 (c) and (d).

Most of the symbols in this work are put in the form, M_{γ}^{δ}, where M stands for a parameter/quantity, while a capital letter is used in place of M for an electrical parameter, a small letter is used for a thermal parameter, as given in Table 3.1. The subscript γ, if it exists, stands for node/section number. The superscript δ, if it exists, stands for the type of the layer ('c'- for conductor, 'cs' for conductor screen, 'i' - for insulation, 'is'- for insulation screen, 'wr'- for water resistant layer, 'sh'- for Al sheath, 'os'- for polyethylene (PE) outer serving and 'su'- for surrounding medium as shown in Fig. 3.2).

TABLE 3.1. Nomenclature of Circuit Parameters

Letter in place of M	The quantity it stands for
k	Thermal conductivity at 293 K $(W/(m.K))$
α	Coefficient of thermal conductivity in $(W/(m.K^2))$
r	Thermal resistance (K/W)
c	Thermal capacitance (J/K)
s	Specific heat capacity in $(J/(kg.K))$
ρ	Mass density (kg/m^3)
i	Thermal current source (W)
R	Electrical resistance (Ω)
C	Electrical capacitance (F)
I	Electrical current (A)

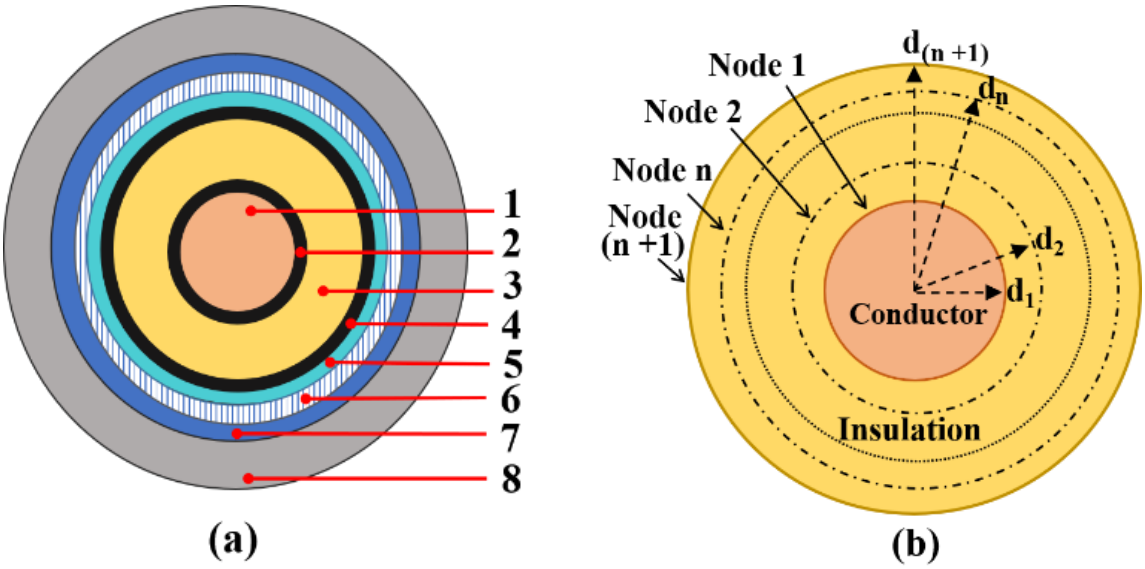

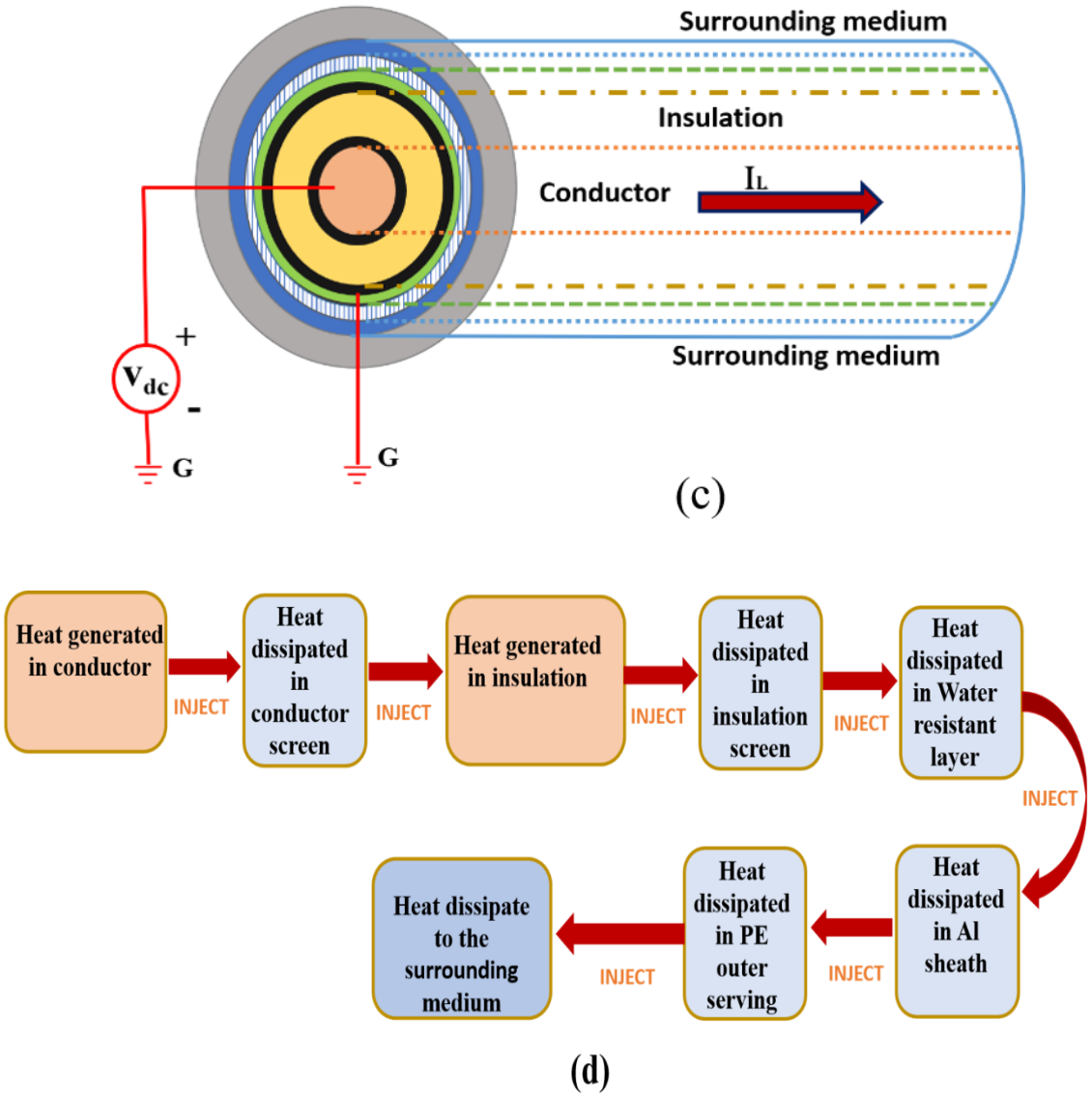

Fig.3.1. (a) Sectional view of buried HVDC cable (C1) used in simulation (1-conductor (Cu-12.6 mm), 2-conductor screen (2 mm), 3-insulation (XLPE-12 mm), 4-insulation screen (1.5 mm), 5-water resistant layer (5.7mm), 6-aluminium sheath (2.3 mm) 7- PE outer serving (5 mm) and 8-soil (1 m). (b) Depiction of concentric cylinders of insulation with increasing radii from d_1 to d_{n+1} and respective node 1 to node n+1, (c) a HVDC Cable in operation , (d) Heat flow direction in cable.

3.2.2 Thermal Resistance and Capacitances

Referring to Fig. 3.2, in the thermal circuit of the cable, the thermal resistances and capacitances have similar connotations in all layers of the cable. Thermal resistance r_γ^δ of a concentric cylindrical strip between nodes γ and $\gamma + 1$, of unit axial length, with inner radius 'd_γ', outer radius '$d_{\gamma+1}$', is,

$$r_\gamma^\delta = \frac{log\left(\frac{d_{\gamma+1}}{d_\gamma}\right)}{2\pi k_\gamma^\delta} \tag{3.1}$$

The variation of the thermal conductivity with temperature v is taken into account by,

$$k_\gamma^\delta = k^\delta + \alpha^\delta \left(v_\gamma^\delta - 293\right) \tag{3.2}$$

The thermal capacitance per unit length c_γ^δ of the strip is calculated by,

$$c_\gamma^\delta = \pi \left[\left(d_{\gamma+1}\right)^2 - \left(d_\gamma\right)^2\right] \rho^\delta s^\delta \tag{3.3}$$

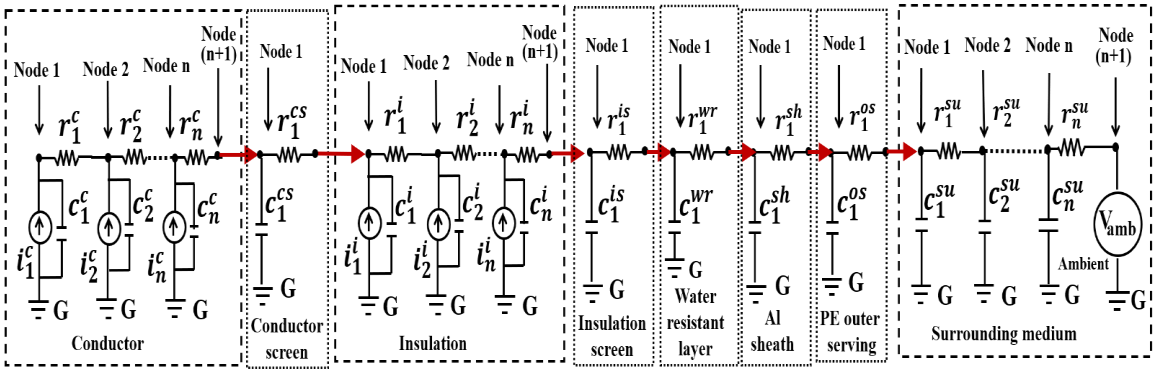

Fig.3.2. Thermal circuit of a cable with all layers and surrounding medium.

3.2.3 Distributed Heat Sources

1) Heat Sources in Conductor: Heat generated inside the body of the conductor, in each strip, has been represented by an equivalent current source in the thermal circuit,

$$i_\gamma^c = \left(I_\gamma^c\right)^2 R_\gamma^c \tag{3.4}$$

where, I_γ^c is axial electrical current through the strip of axial resistance R_γ^c, defined in the next sections.

2) Heat Sources of Insulation: Heat generated inside an insulation strip has been represented by an equivalent current source,

$$i_\gamma^i = \left(I_\gamma^i\right)^2 R_\gamma^i \tag{3.5}$$

where I_γ^i, is the radial electric current through the radial electric resistance of the strip R_γ^i, which is nonlinear and has been accurately incorporated in this work (depending on electrical and thermal quantities), described in the next sections. Absence of heat sources within the surrounding earth allows us to neglect the equivalent current sources in the soil.

3.2.4 Electrical Circuit of Conductor

The electrical circuit of conductor can be modeled as a distributed parameter network as shown in Fig. 3.3 (a). Each of the resistances correspond to the respective axial resistance of each strip of unit length, the variation of whose electrical resistivity with temperature is incorporated, given by,

$$R_\gamma^c = \frac{\rho_0\left(1+\alpha\left(\frac{v_\gamma + v_{\gamma+1}}{2} - 293\right)\right)}{\pi\left(\left(d_{\gamma+1}\right)^2 - \left(d_\gamma\right)^2\right)} \tag{3.6}$$

Where, ρ_0 electrical resistivity at $293K$ and α temperature coefficient of resistivity of conductor in (K^{-1}). The strip temperature is taken as average of node temperatures, v_γ and $v_{\gamma+1}$ of conductor thermal circuit.

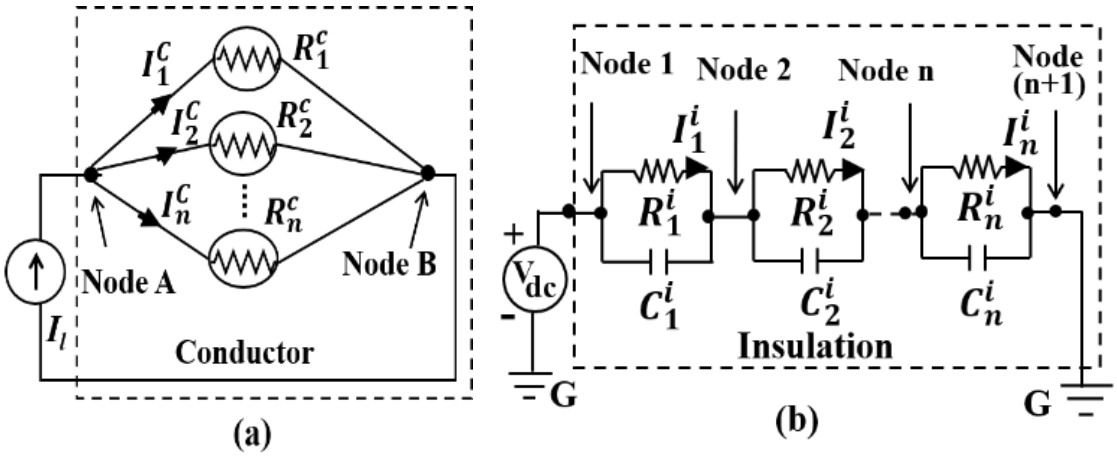

Fig.3.3. Electrical circuit of (a) Conductor, (b) Insulation.

3.2.5 Electrical Circuit of Insulation

The electrical circuit of insulation is modeled as a distributed network with combination of insulation resistor and in parallel with capacitor is shown in Fig. 3.3 (b). Also, the applied electric stress to the cable has been represented by a corresponding voltage source (V_{dc}).

1) Electrical Resistances: For the insulation, the electrical resistance of a cylindrical strip of unit length is,

$$R_\gamma^i = \frac{\log\left(\frac{d_{\gamma+1}}{d_\gamma}\right)}{2\pi\sigma} \tag{3.7}$$

Electric field and temperature dependence of insulation conductivity σ is considered for electric conductivity [26], [27] by,

$$\sigma = Ae^{\left(\frac{-b}{T} + a|E|\right)} \tag{3.8}$$

Where, A is the conductivity coefficient of insulation (S/m), a is stress coefficient (m/V), b is the temperature coefficient (K). Temperature within insulation is given by the voltage of the thermal circuit, v_γ at a node γ of the dielectric thermal circuit. Hence, using (27) and (28), electrical resistance of a cylindrical strip of unit length in insulation is given by,

$$R_\gamma^i = \frac{\log\left(\frac{d_{\gamma+1}}{d_\gamma}\right) e^{\left(\frac{b}{v_\gamma} - a|E_\gamma|\right)}}{2\pi A} \tag{3.9}$$

Now, electric field E_γ in the strip can be estimated as,

$$E_\gamma \approx \frac{V_\gamma - V_{\gamma+1}}{(d_{\gamma+1} - d_\gamma)} \tag{3.10}$$

Substituting in (3.10),

$$R_\gamma^i = \frac{\log\left(\frac{d_{\gamma+1}}{d_\gamma}\right) e^{\left(\frac{b}{v_\gamma} - a\left|\frac{V_\gamma - V_{\gamma+1}}{(d_{\gamma+1} - d_\gamma)}\right|\right)}}{2\pi A} \tag{3.11}$$

2). Electrical Capacitances: The electrical capacitance of each insulating cylindrical strip of unit length, with outer radius '$d_{\gamma+1}$', inner radius 'd_γ', vacuum permittivity ε_0 and relative permittivity ε_r, is given by,

$$C_\gamma^i = \frac{2\pi\varepsilon_0\varepsilon_r}{\log\left(\frac{d_{\gamma+1}}{d_\gamma}\right)} \tag{3.12}$$

The above circuit models have been used for simulation of electro-thermal phenomenon in various cables as mentioned in the following section.

3.3 Cables used in Simulations and Validation

A 400 MW, bipolar, $\pm 200\ kV$, 500 mm^2, HVDC cable (C1) of a local vendor, with various layers as shown in Fig. 3.1, is considered for simulation of electric field, temperature, thermal runaway (breakdown) and other results, such as effect of load current. The PSPICE software is used for the simulation. The physical parameters of the power cable system used in the simulation are listed in Table 3.2.

In view of the significance of thermal runaway, three more types of cables, C2, C3 and C4 are used for the validation of the proposed circuit models with experimental results.

TABLE 3.2 Physical Parameters of Power Cable (C1) [21, 22, 35]

Quantity	Value	Quantity	Value
k^c	413 $(W/(m.K))$	k^{soil}	2.1 $(W/(m.K))$
α^c	-0.06 $(W/(m.K^2))$	s^{soil}	700 $(J/(kg.K))$
ρ^c	8960 (kg/m^3)	ρ_0	2.65 x 10^{-8} $(\Omega.m)$
s^c	390 $(J/(kg.K))$	α	0.0039 (K^{-1})
k^i	0.33 $(W/(m.K))$	k^{oil}	0.11 $(W/(m.K))$
α^i	-1.53 x 10^{-4} $\left(\frac{W}{m.K^2}\right)$	s^{oil}	1860 $(J/(kg.K))$
ρ^i	920 (kg/m^3)	ρ^{oil}	877 (kg/m^3)
s^i	2200 $(J/(kg.K))$	A	2×10^{-11} $\left(\mathrm{S}/\mathrm{m}\right)$
ε_0	8.854x 10^{-12} $\left(\mathrm{F}/m\right)$	a	7×10^{-08} $\left(\mathrm{m}/\mathrm{V}\right)$
ε_r	2.25	b	3.7×10^3 K
ρ^{soil}	2270 (kg/m^3)	l	1 (m)

The cables of type C2 used for experiments in author' lab have a solid copper conductor of $6\,mm^2$, XLPE insulation thickness of $0.7\,mm$ and rated voltage of $1100\,V$, manufactured as per IS standard [36]. Leakage current and thermal runaway experiments as detailed in the next section, are conducted on these cables.

The cables of type C3 [38], had $200\,mm^2$ conductor and XLPE insulation thickness of $9\,mm$, with two sub-types of XLPE for ac and dc materials. The cables of type C4 by S. Ogata [39], had three sub-types, Type I, Type II and Type III, as shown in Table 3.3.

TABLE 3.3 Cable Parameters of C4 (S. Ogata [39])

Item	Value		
	Type I	Type II	Type III
Conductor size (mm^2)	200	200	500
XLPE Insulation thickness (mm)	2.5	9.0	13.0

3.4 Results and Discussion

Simultaneous simulation of inter-dependent circuit models was performed in a circuit simulation environment for C1, for unit axial length of the cable. Electric field, temperature, thermal runaway (breakdown) and other results such as the effect of load current are presented and discussed.

3.4.1 Simulation of Electric Field and Temperature Profile

Results of temperature and electric field distribution in insulation, at different times after switch on, are shown in Figs. 3.4 and 3.5 respectively, for the cable (C1) switched on at full load. Time taken to reach almost steady-state is observed to be nearly 3 days. It can be seen that the temperature stabilization takes longer time, than the electric field. This happens due to the differences in stabilization times of temperature, T (Fig. 3.6) and the value of $\triangle T$ (Fig. 3.7). The $\triangle T$ which determines electric field, stabilizes faster than T. It can be seen that, the profiles of steady-state electric field and temperature are in conformity with the earlier works [23], [26].

Effects of load current on steady-state electric field and temperature are shown in Figs. 3.8 and 3.9 respectively. The phenomenon of stress inversion can be observed at higher load currents. However, the maximum field at full load is not high when compared to the no load case.

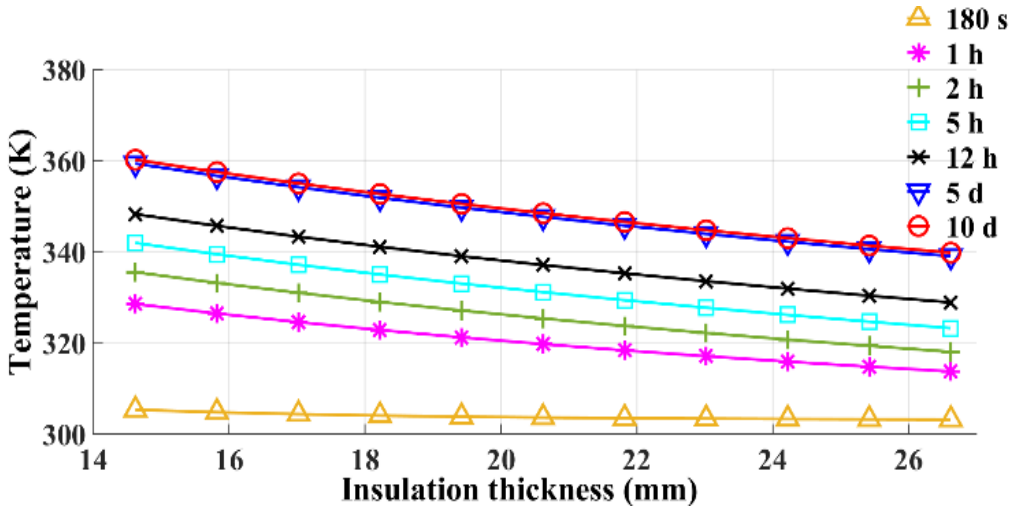

Fig.3.4. Temperature distribution across cable insulation at full load for different time instants after switch on. The temperature rises relatively fast initially but takes considerable time to stabilize.

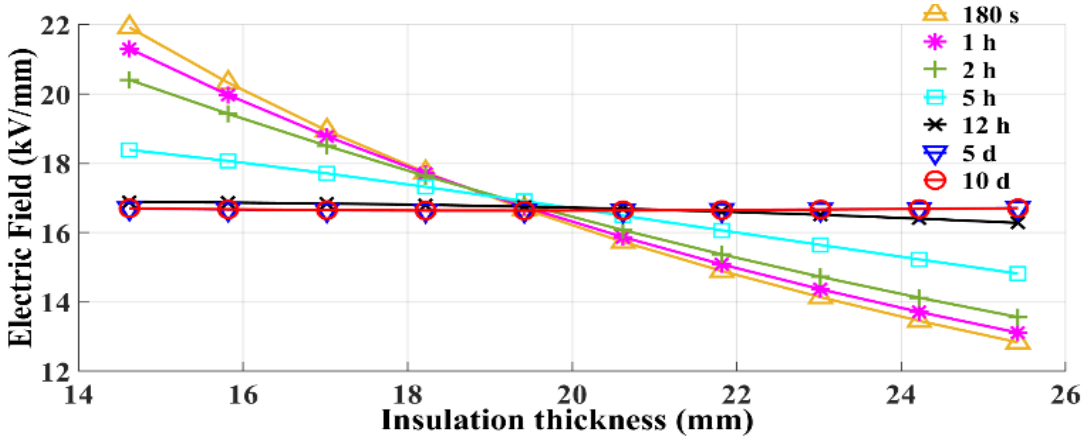

Fig.3.5. Electric field distribution across cable insulation at full load for different time instants after switch on. The stabilization time is relatively less than in the case of temperature distribution.

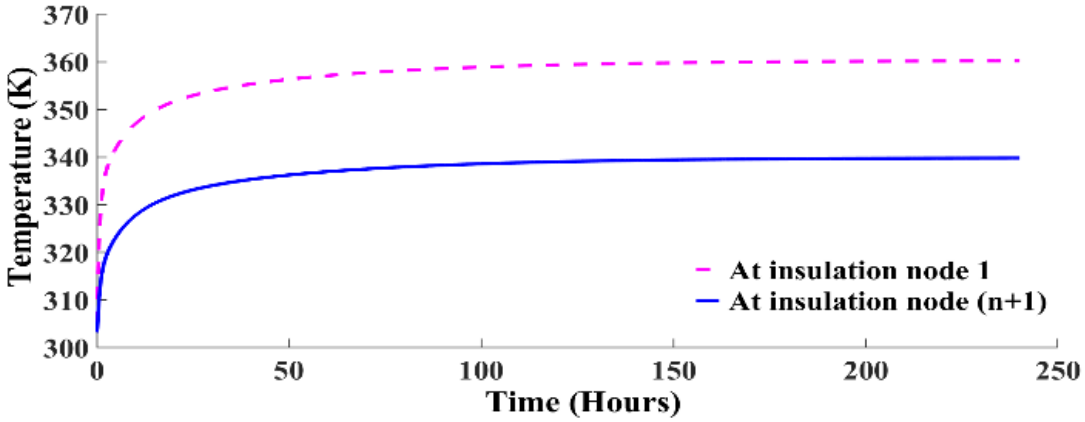

Fig.3.6. Boundary temperatures of insulation after switch on at full load. It takes similar time for both boundary temperatures to stabilize.

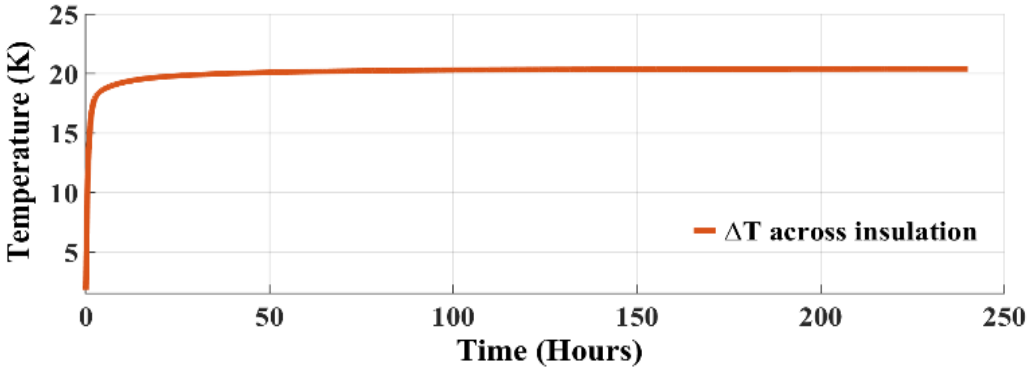

Fig.3.7. Temperature difference (ΔT) across insulation after switch on at full load. The stabilization time is comparatively little in contrast to that of temperature distribution, which also reflects in the electric field distribution which depends on ΔT.

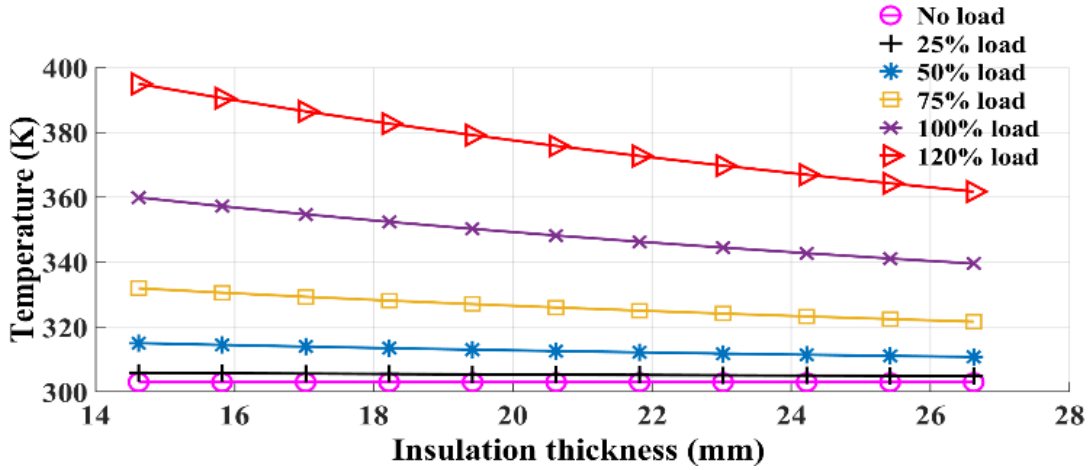

Fig.3.8. Steady-state temperature distribution in insulation for different load currents. As the load increases, insulation boundary near the conductor gets increasingly thermally stressed.

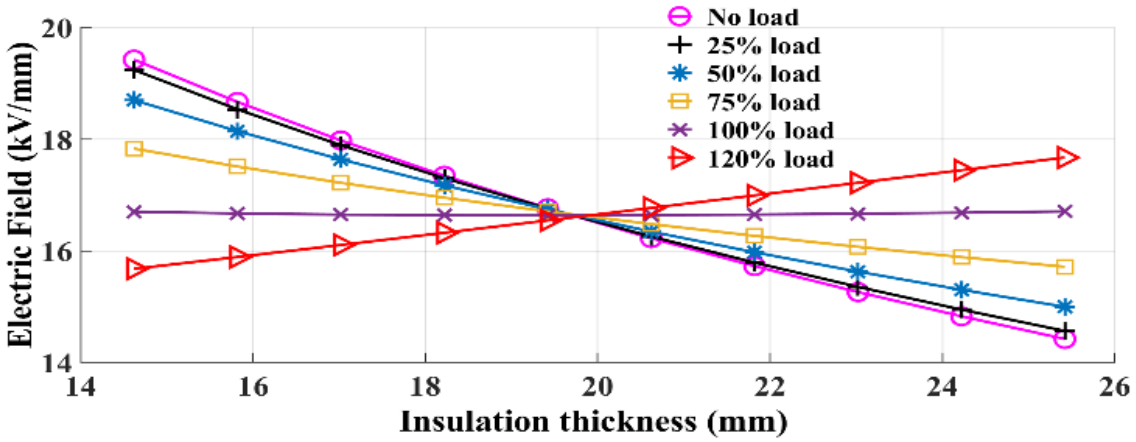

Fig.3.9. Steady-state electric field distribution in insulation for different load currents. The field distribution tends to be uniform with increasing load, however, beyond certain load, it becomes non-uniform again.

3.4.2 Field and Temperature during a Load Cycle

Electric field distribution in cable insulation during a typical load cycle of heating for 240 hours (load) followed by natural cooling (no-load) for 240 hours, is shown in Fig. 3.10. The corresponding temperature distribution is shown in Fig. 3.11.

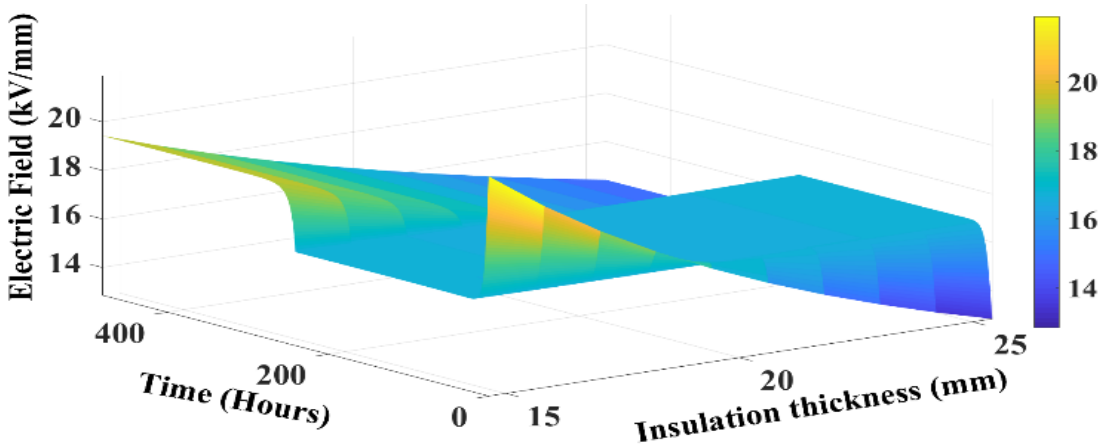

Fig.3.10. Electric field distribution in insulation during load cycle. At the switch-on instant, the peak electric field tends to be very high due to Laplacian Distribution.

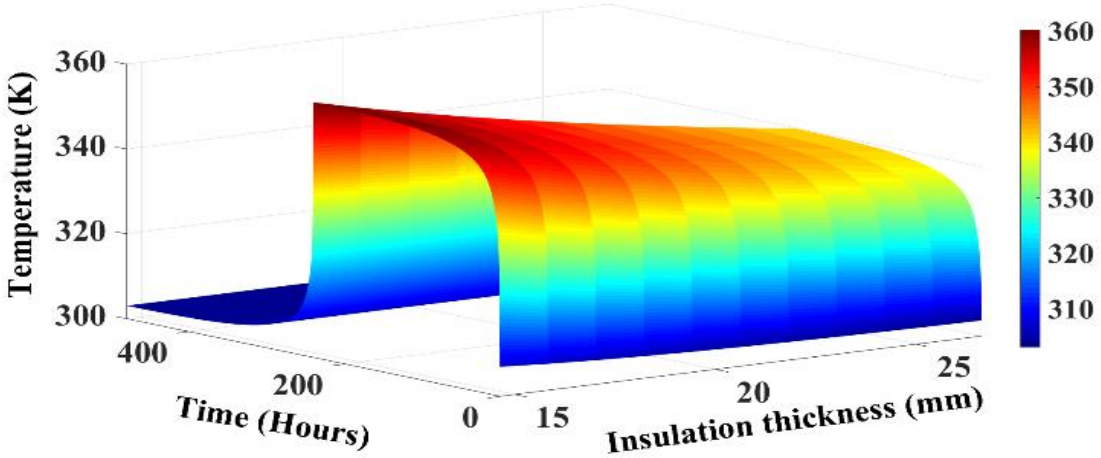

Fig.3.11. Temperature distribution in insulation during load cycle. The insulation is subjected to maximum thermal stress during heating cycle.

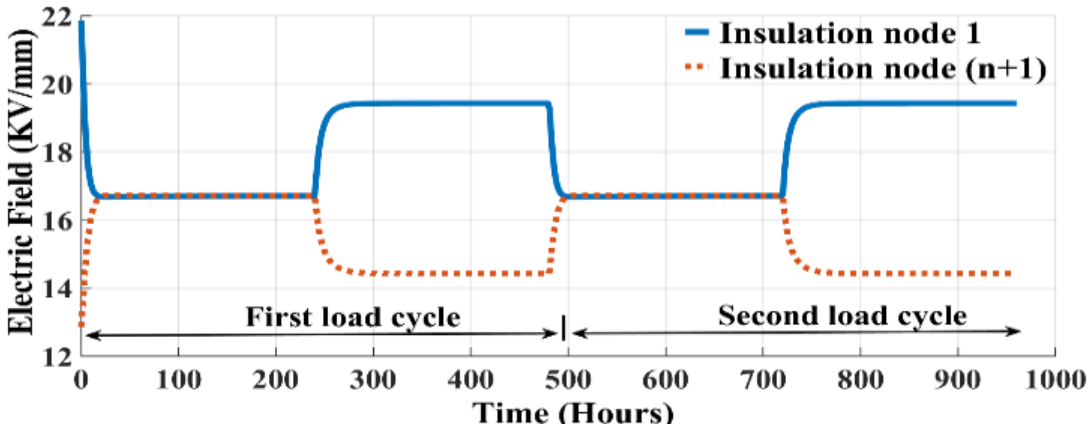

Fig.3.12. Boundary electric fields of insulation during load cycle. The peak electric field is present immediately after switch on, in the first load cycle.

Referring to Fig. 3.12, the peak electric field in insulation immediately after switch on is high due to Laplacian distribution (field at time t = 0 in Fig. 3.12), during the first load cycle. The peak electric field will never be this high subsequently as the resistive distribution comes into effect under dc with its corresponding space charge distribution. The maximum and minimum field in insulation changes dynamically with temperature variation in subsequent load cycles, due to field and temperature dependent resistivity of insulation medium.

3.4.3 Simulation of Breakdown of Power Cable

While the above results are interesting, the main contribution of this work is in the simulation of electro-thermal runaway or breakdown of a cable. The dynamic change in electric field profile of C1 under full load until breakdown after a step voltage of 1870 kV is applied is shown in Fig. 3.13. Its corresponding temperature distribution is shown in Fig. 3.14. The field immediately after the voltage is turned on is Laplacian and becomes resistive (Poisson's) in a short time and continues to be resistively graded while exhibiting dynamic changes near breakdown. The ambient temperature is taken as $30°C$. The peak temperature and electric field in the insulation increase drastically before breakdown, indicating that even in thermal breakdown electric field increases before breakdown.

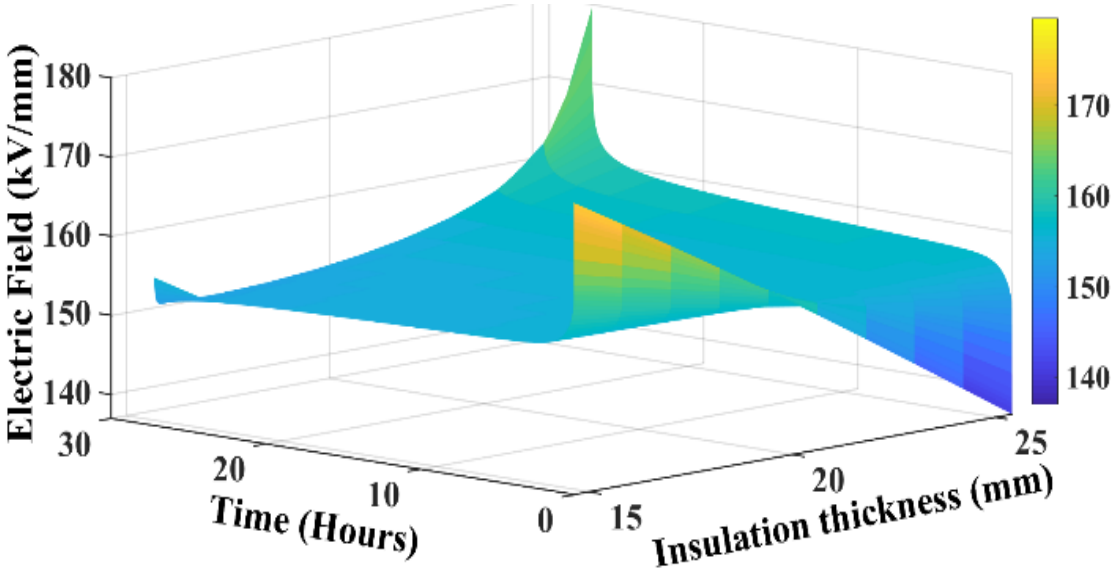

Fig.3.13. Electric field distribution in insulation after switch on, till breakdown, at 1870 kV. Runaway in field at ends of insulation with peak at outer insulation surface, while dip in the middle of the insulation is observed, depicting the hetero charge formation near the breakdown.

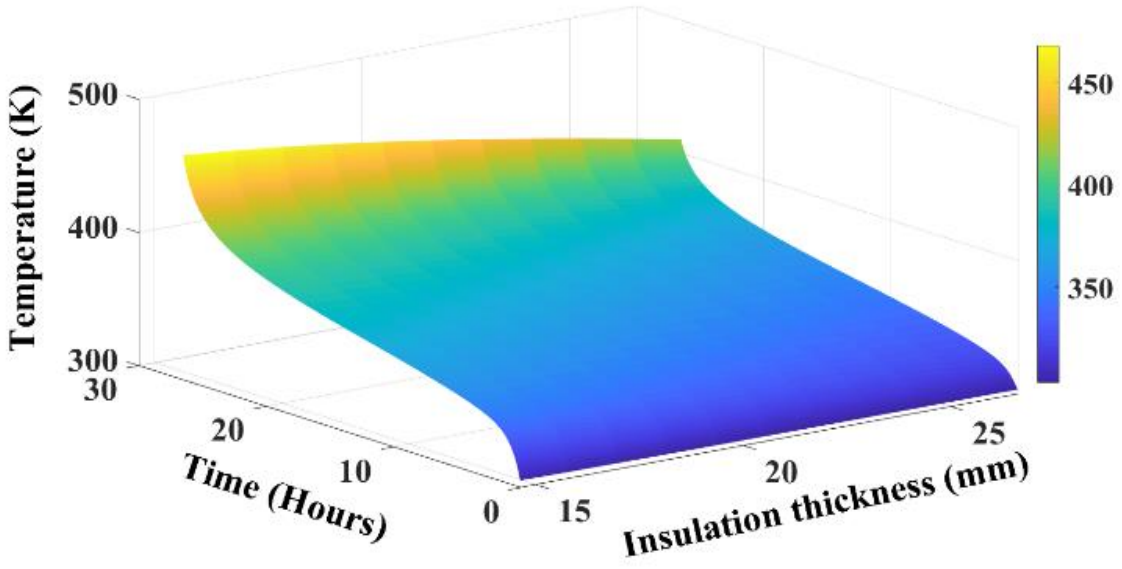

Fig.3.14. Temperature distribution in insulation, after switch on, till breakdown, at 1870 kV. Runaway in temperature with peak near the conductor before breakdown.

The leakage current, hot-spot temperature and peak electric field, are plotted in Figs. 3.15, 3.16 and 3.17 respectively, for four different voltages. The leakage current magnitude is about $5.54 \times 10^{-5} A$, $7.46 \times 10^{-5}\ A$ and $8.40 \times 10^{-5} A$ and the electric field is about $152\ kV/mm$, $155\ kV/mm$ and $163\ kV/mm$ during breakdown for applied voltages of $1770\ kV$, $1800\ kV$ and $1870\ kV$ respectively.

The time-to-breakdown and effect of load current on breakdown voltage is shown in Fig. 3.18, with a single step voltage application of various voltage magnitudes. It is important to notice that the initial portion of the characteristics (< ~1 hour) looks linear and similar to volt-time (life) characteristics, but there is no ageing effect involved in the circuits. Therefore, it is the characteristics of the 'transient thermal breakdown', in which the breakdown occurs before a steady-state could be normally arrived and hence the load current has no effect in this case.

When the voltage magnitude is decreased, the time to breakdown increases, and for larger times to breakdown, the effect of load current on breakdown voltage becomes visible, due to rise in temperature due to external thermal resistance. For a critical voltage magnitude, referred to as steady-state thermal maximum voltage V_{th} by Whitehead [27], the thermal runaway will not occur. Clearly the V_{th} is dependent on load current as predicted in earlier works on steady-state thermal limits with external heat injection [24], [25].

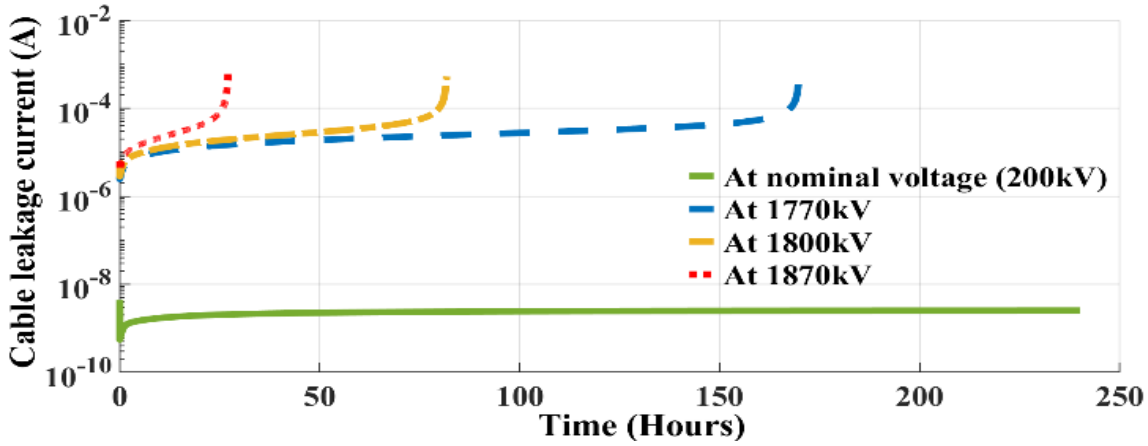

Fig.3.15. Runaway of leakage current at different voltages for loaded cable.

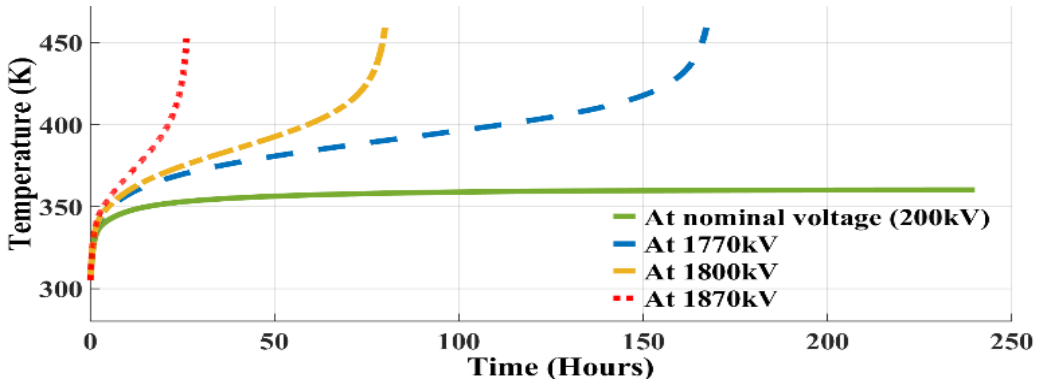

Fig.3.16. Runaway of hot-spot temperature at different voltages for loaded cable.

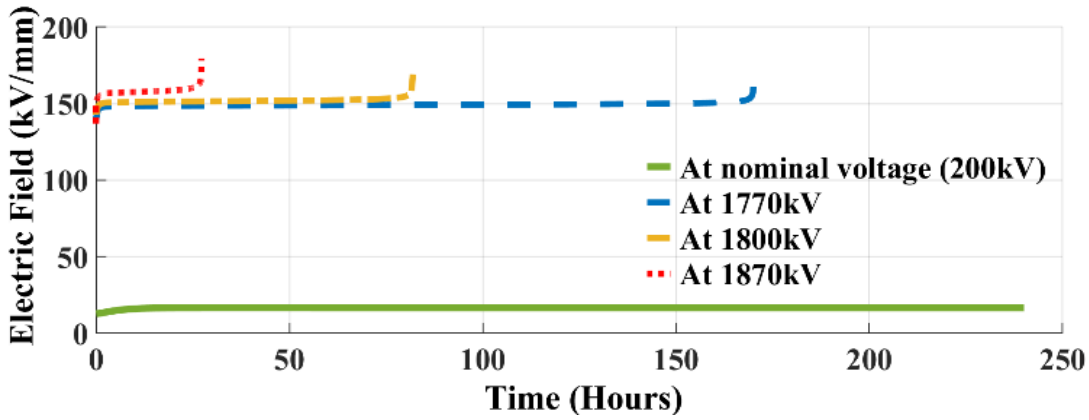

Fig.3.17. Runaway of peak-electric field at different voltages for loaded cable

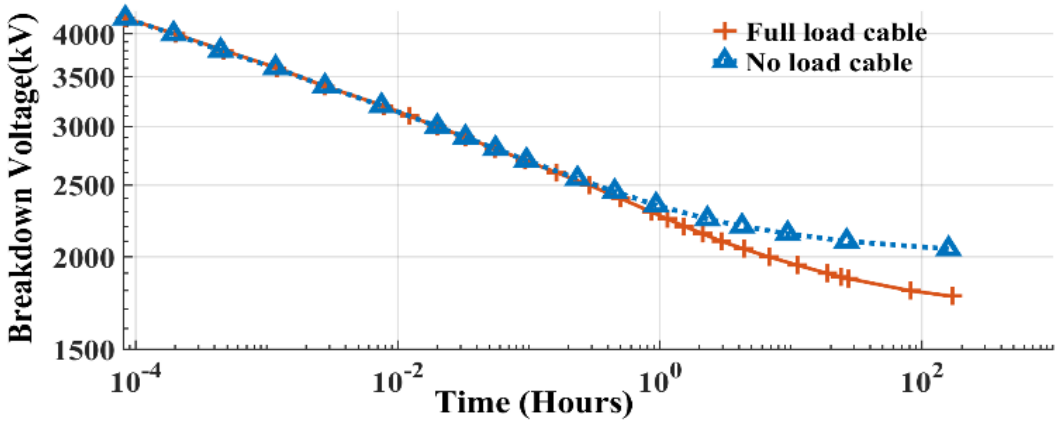

Fig.3.18. Simulation of voltage vs time to breakdown characteristics for cable under no load and loaded conditions. The effect of load current is seen only for breakdown at lower voltages or larger times to breakdown. This plot delineates interactive and intrinsic breakdown phenomena.

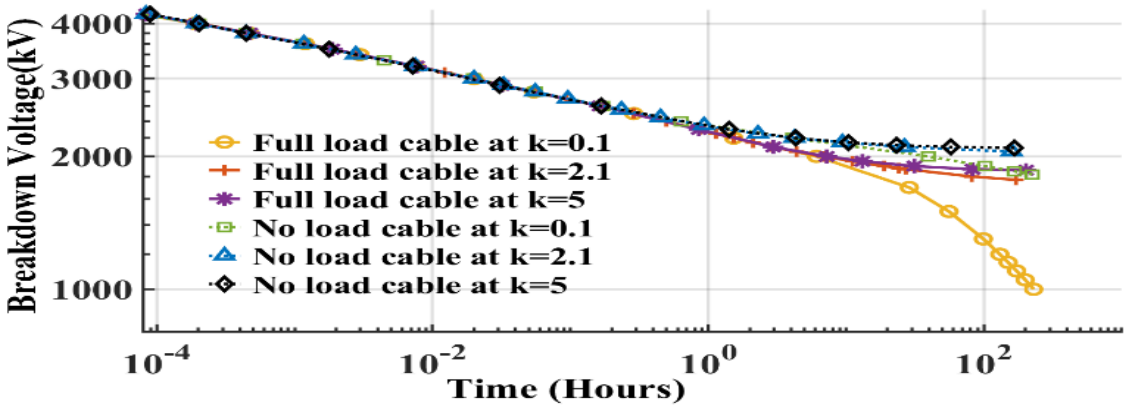

Fig.3.19. Simulation of voltage vs time to breakdown characteristics at different soil thermal conductivities (or different external thermal resistances of backfill) under no load and loaded conditions.

Effect of external (soil) thermal resistance is shown in the Fig. 3.19. The constant sheath temperature case corresponds to zero thermal resistance (or infinite thermal conductivity) and can be seen to be having the highest thermal breakdown voltage. The ensuing thermal runaway is *not* due to interaction with the external thermal resistance but due to the cascading positive feedback in the insulation arising out of non-linear conductivity referred to as internal thermal breakdown or intrinsic thermal breakdown [24]. The rest of the cases correspond to non-zero thermal resistance. For the loaded cable, the steady-state breakdown voltage is seen to stabilize for a given external thermal resistance, until the value corresponding to a thermal conductivity (k) of 2.1 W/mK, as can be seen in Fig. 3.19.

However, for any further increase in thermal resistance, the slope of the characteristics turns negative, indicating a runaway even at lower voltages. Of course, the time to breakdown increases with decreasing voltage. This is referred to as interactive thermal breakdown as this is due to failure of heat exchange to environment [24]. Therefore, the back-fill of cable assumes huge significance for normal functioning of the cable and even a short length of high thermal resistance along the cable would trigger breakdown due to interactive thermal breakdown.

3.5 Validation of Proposed Models with Experiments

The proposed models are validated with experiments conducted in author's lab as well as with those available in the literature. The experiments were conducted on cables of type C2 in author' laboratory. The details of experiments are given below.

3.5.1 Experiments on Conduction Current Measurement

The volumetric current through the insulation is measured to find out volumetric resistivity of cable [37] and A, b and a parameters of σ, using a cylindrical 3-terminal electrode system. The tests were conducted for three electric fields: $10\ kV/mm$, $20\ kV/mm$, $30\ kV/mm$, each at three different temperatures: $323\ K$, $343\ K$ and $363\ K$ for five samples. The geometric mean of the experimentally measured leakage currents is plotted in Fig. 3.22. The A, a, b coefficients are thus obtained experimentally, as: 11.34, $1.01\text{x}\ 10^{-7}$ and $1.17\ \text{x}\ 10^{4}$ respectively in SI units.

3.5.2 Experimental Setup for Breakdown Tests on Loaded Cables

The breakdown voltage of the XLPE cable (C2) was experimentally determined using a setup shown in Fig. 3.20, whose primary components are: a current transformer (CT), a hot air oven, a specially designed HV electrode and a HVDC source. The CT primary is connected across the two ends of the test cable conductor (marked as input and output in Fig. 3.20) and the secondary is connected across a variac, by adjusting which, different load currents are circulated in the test cable, using induction principle (as direct circulation requires a low voltage source with high current rating). The cable is connected in a closed loop to circulate different load current in the cable.

The oven was used to maintain controlled environmental temperatures. In which different temperature can be archived in the cable insulation. The HV electrode is made up of brass, and has a cylindrical shape in the centre and a conical shape at the ends. The central diameter is chosen such that the outer layer of the cable insulation touches it, while the conical shape at the ends is chosen to avoid the edge breakdown (due to the high electric stress present at the edges).

The front and top view of the HV electrode as well as a punctured XLPE cable is shown in Fig.3.21. High voltage is applied to this electrode using a HVDC source, while the cable conductor is grounded. The test cable is placed in transformer oil to avoid flashover, because the oil breakdown strength is high compared to air. The simultaneous application of high voltage and load current to the test cable subjects it to different electro-thermal stress. This test setup help to apply different electro-thermal, environmental stress to the cable insulation medium.

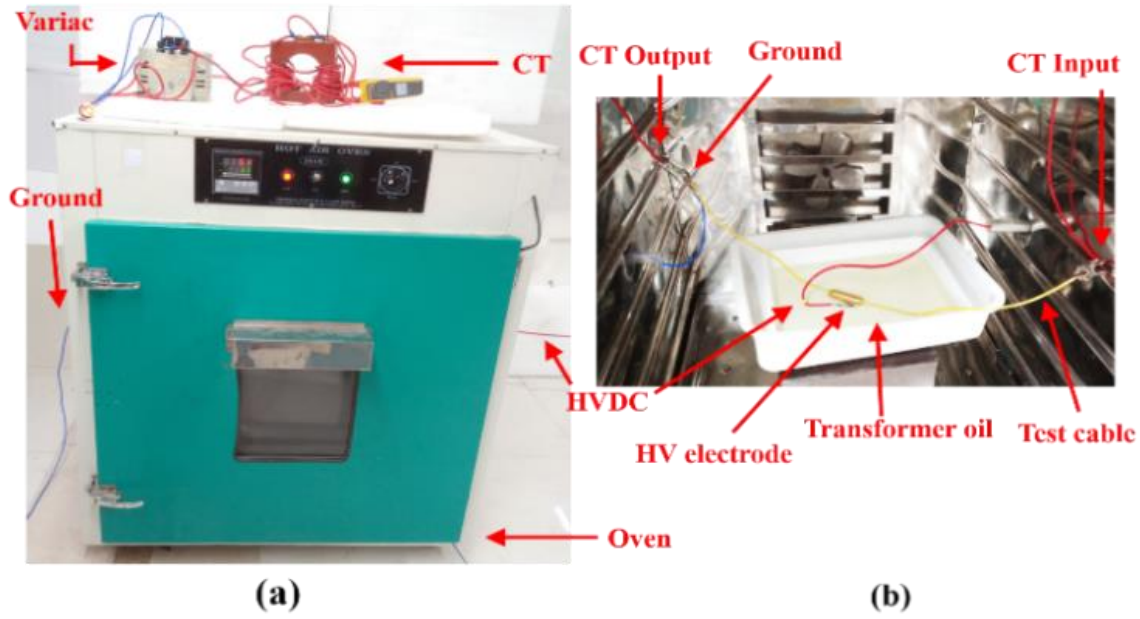

Fig.3.20. (a) Experimental setup for electro-thermal breakdown, (b) inside view of the oven.

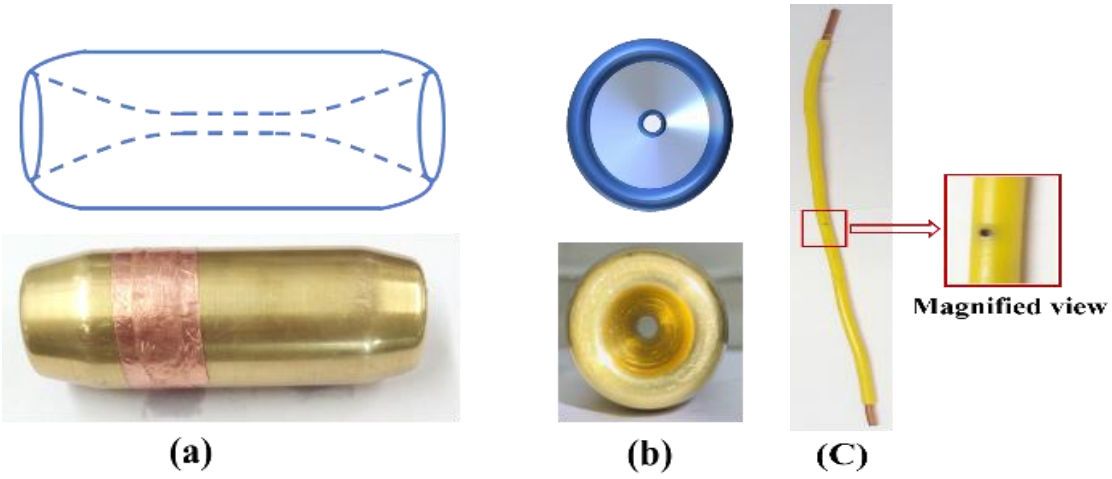

Fig.3.21. Special high voltage electrode used for cable breakdown (a) top view, (b) front view. (c) Punctured XLPE cable.

Before conducting the breakdown tests, XLPE cable samples were preheated in oven at 80°C for 48 hours to remove moisture from sample. The voltage is increased with a step of 2 kV/min until breakdown, for all tests at different load currents. A total of 60 cable samples were tested.

3.5.3 Validation with Experiments on Cables C2

Referring to Fig. 3.22, the simulated conduction/leakage current in insulation of C2 is in good agreement with geometric mean of the experimental results. The 2-parameter Weibull distribution plots of cable breakdown under full load and no load for different temperatures is shown in Fig. 3.23. Referring to Fig. 3.24, the Weibull scale parameters (63.2% probable breakdown voltage) of experimental breakdown voltage reasonably match with simulations for both loaded and no-load cases. The error is less than 11.60% and Pearson correlation coefficient is ~1 for unloaded cable at different temperatures. The error is less than 12.27% and Pearson correlation coefficient is ~1 for different load currents, in case of loaded cable. The 95% confidence intervals are also shown in the same plot.

3.5.4 Validation with Experimental Results of C3 and C4.

Referring to Fig. 3.25 (a), the dc breakdown voltages for both AC-XLPE and DC-XLPE cables of C3 [38] are in reasonable agreement with simulated results using the volume resistivity and other parameters provided in [38]. The error is less than 7.40%.

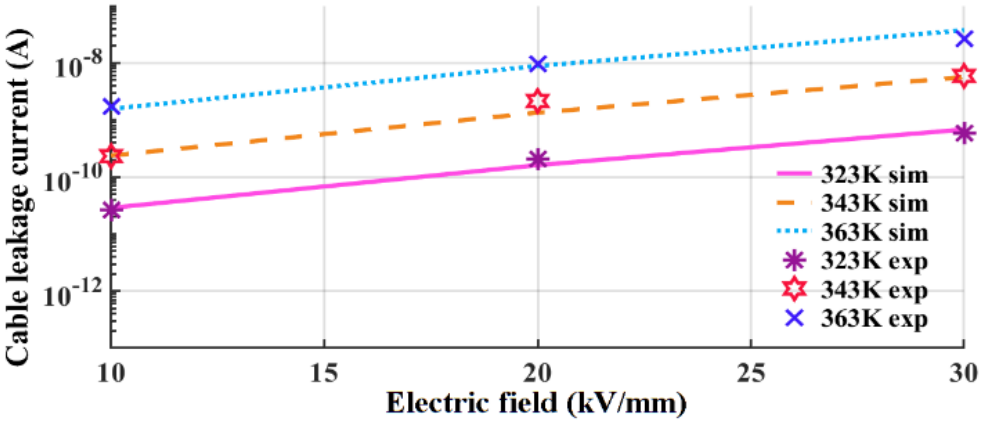

Fig.3.22.Comparison of simulated and experimental (geometric mean) leakage currents at different electric fields and temperatures (C2).

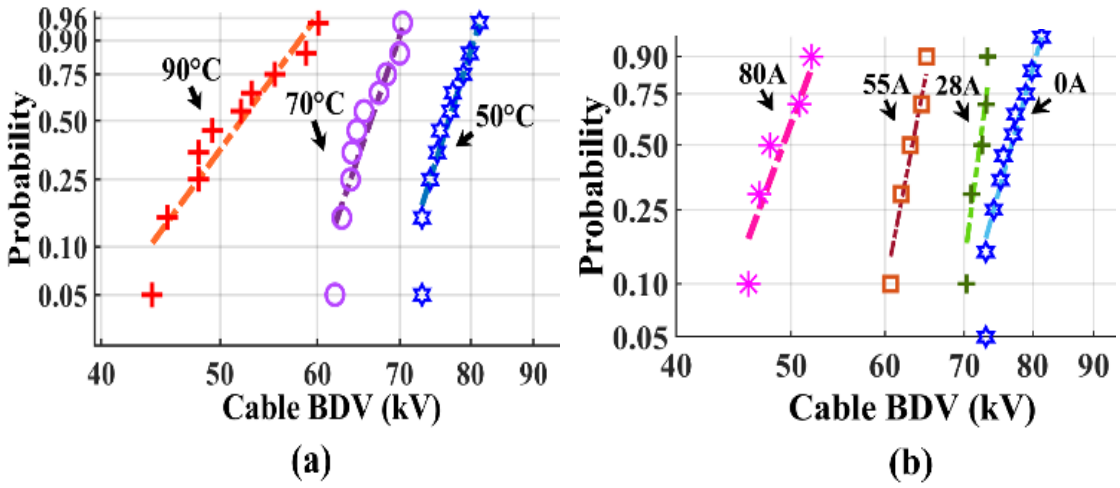

Fig.3.23. 2-parameter Weibull distribution plots of experimental breakdown voltage of cables (C2) (a) at different temperatures under no load, (b) at different load currents with constant ambient temperature of 50°C.

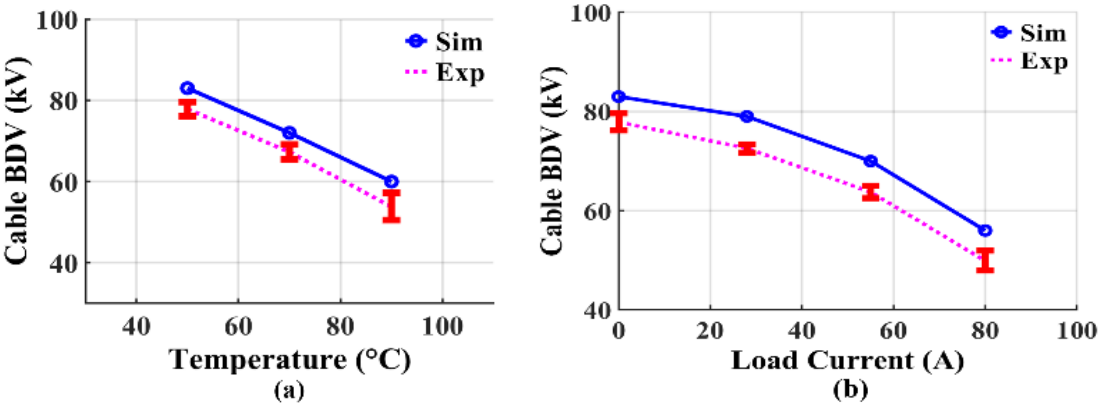

Fig.3.24. Comparison of 63.2% experimental breakdown voltages with simulations (a) under no load. (b) under different load currents at constant ambient temperature of 50°C.

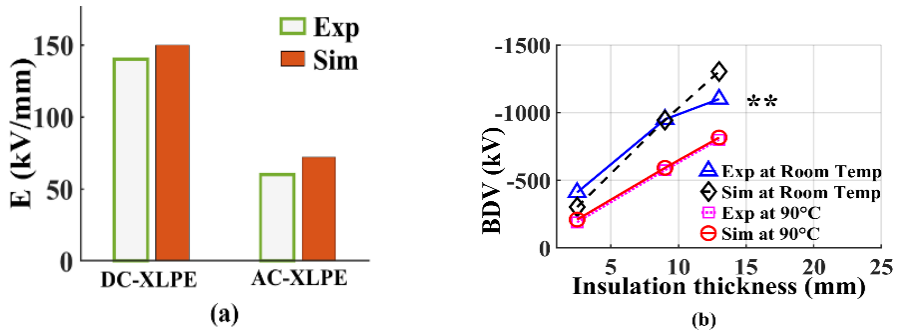

Fig.3.25. Comparison of simulations with experimental breakdown voltages for (a) Cables of C3 [18], (b) Cables of C4 [19].

For the cables of C4, predicted thermal breakdown voltages using test conditions of [39] are close to experimental results as shown in Fig. 3.25 (b). The 13 mm-thick cable data marked by asterisks (**) corresponds to edge breakdown as reported in [39]. It has been found to be $-1304\,kV$ using simulations. Apart from other results, this proves the importance of the simulations proposed in the work.

3.5.5 Validation with FEM Simulations

The results of the proposed model are compared with FEM simulations for the power cable C1 for the case of full load current. Dirichlet boundary condition of electric potential are applied at the conductor and boundary. In case of thermal boundary conditions, a Neumann condition is used at the conductor boundary while the outer boundary of soil is assumed to be at the ambient temperature (Dirichlet condition). The electric field distribution at thermal runaway is shown in Fig. 3.26.

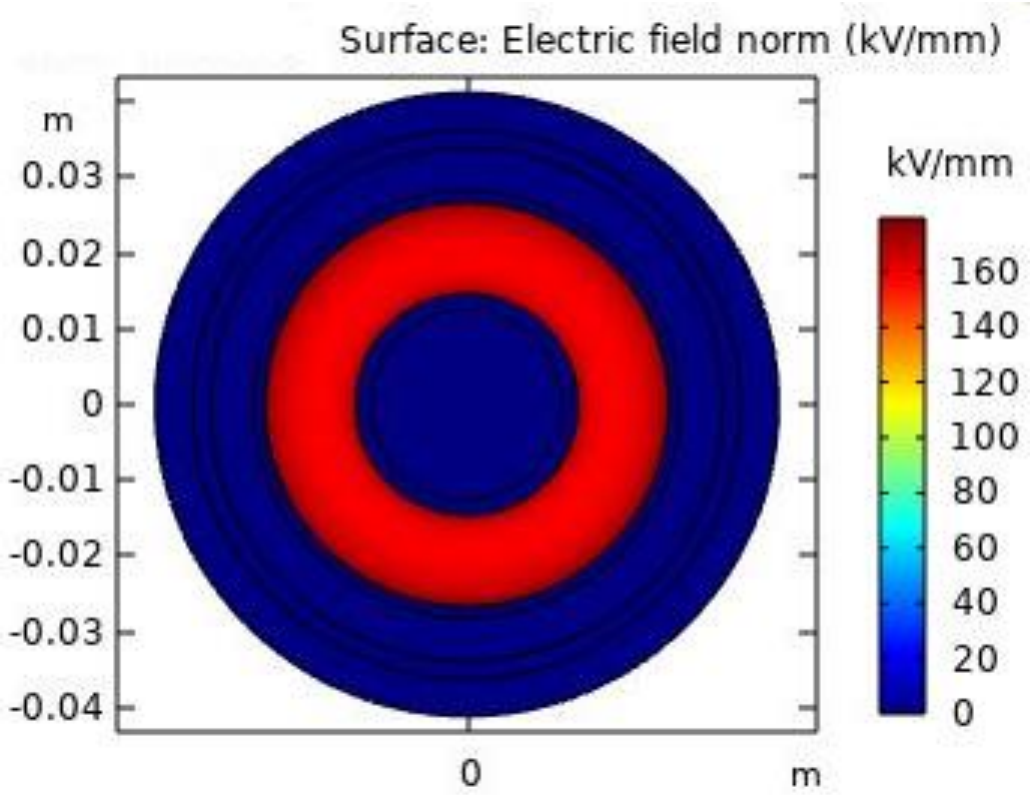

Fig.3.26.Electric field distribution in insulation at 2000 kV.

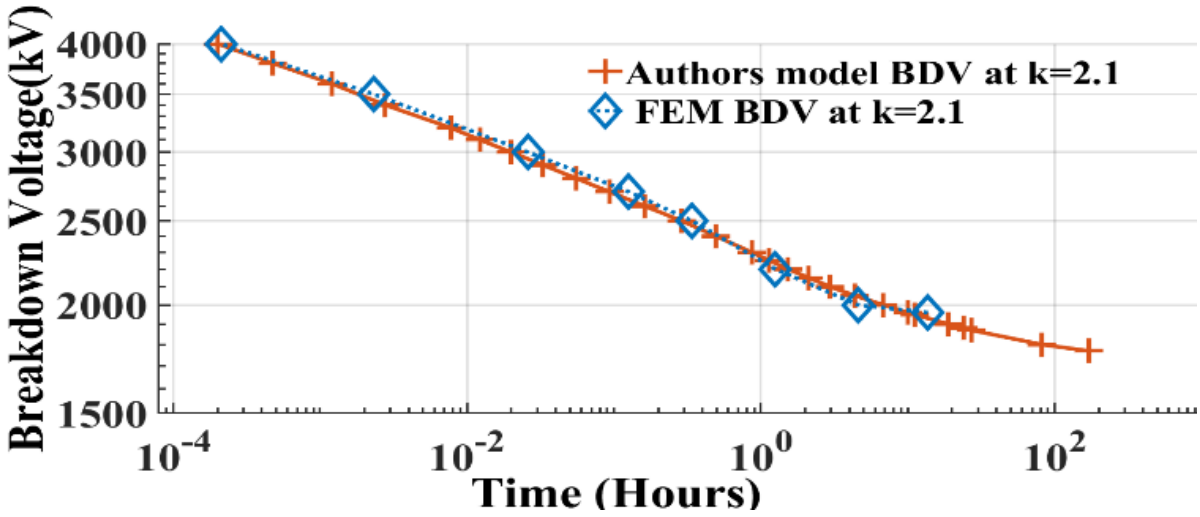

Fig.3.27. Comparison of voltage vs time to breakdown characteristics of circuit model with FEM model.

The voltage vs time characteristics is also compared in Fig. 3.27, and it is in agreement with that obtained using circuit model, as the deviation is less than 2% for breakdown voltage at any time instant. The Pearson correlation coefficient is ~1.

The summary of this chapter presents simulation of electro-thermal runaway and thermal limits of loaded HVDC Cables using circuit models for electrical and thermal phenomena. The runaway of temperature is accompanied by a runaway in peak electric field and conduction current through the dielectric, indicating that even in thermal breakdown, the electric field and the current tend to increase exponentially before breakdown. The zones of internal and interactive thermal breakdown have been delineated in this work, for the first time. Effect of external thermal resistance and hence the effect of back fill on the breakdown is simulated. Often difficulties are encountered in testing loaded cables, and the current work provides an estimation of breakdown voltage based on measurement of physical parameters and load current. Therefore, the present work is believed to be useful for the cable designers. Some important points of work have been presented in conclusions chapter 5. The variation in ambient temperature, load currents, applied voltage and considered 1m soil in simulation may differ simulation from experimental results.

CHAPTER 4

Effect of Long-term Thermal Ageing on Space Charge Dynamics in LDPE

4.1 Introduction

Ageing is a slow but irreversible chemical process which leads to the degradation of dielectric properties of cable insulation. Prolonged thermal stress accelerates the ageing, gradually weakens the insulation and hence ultimately leads to failure. Therefore, investigation on insulation ageing is vital for the optimal design of insulation of high voltage power apparatus, especially cables. One of the main issues of polymeric cables is space charge accumulation under HVDC fields, which is further affected due to ageing of insulation, since the cable operates under continuous thermal stress. While there is ample literature on space charge in fresh and short-term aged samples [46-48], [51-53], and even at breakdown fields (in fresh samples), there is a clear lacuna related to space charge under long-term ageing. In this work, LDPE is thermally aged up to 256 days. The space charge dynamics, electric field, field enhancement factor and net charge in the insulation bulk material are investigated experimentally and interesting results are presented.

4.2 Experimental details

The methodology of sample preparation and various experiments are described in this section.

4.2.1 Sample Preparations

LDPE sheet samples are prepared from granules, supplied by a local cable manufacturing industry, using a two-roll mill at 110℃, followed by pressing in hydraulic press (as shown in Fig. 4.1 (a) and (b)) at temperature and pressure of 120℃ and 90 bar respectively. The thickness of the prepared samples is approximately $100 \pm 10\ \mu m$.

4.2.2. Ageing Experiments

Long-term thermal ageing was carried out in a systematic manner by keeping the prepared sheet samples in batches inside hot air ovens maintained at temperatures of 70℃ and 80℃ for time periods of 32 days, 64 days, 128 days and 256 days. Selected fresh and aged LDPE samples are shown in Fig. 4.1 (c).

(a)

(b)

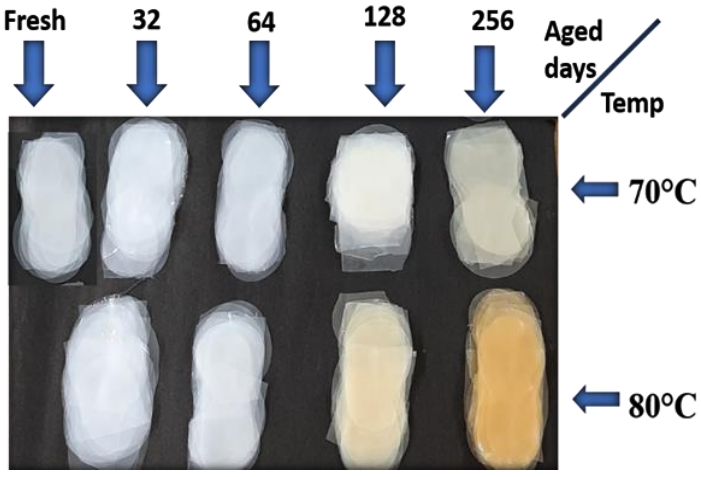

(c)

Fig. 4.1. (a) Two roll mills, (b) Hydraulic press, (c) Fresh and Aged LDPE samples.

4.2.3 Space Charge Measurement Setup (PEA)

A Pulsed Electroacoustic (PEA) setup, as shown in Fig 4.2, has been used for space charge measurements, as per IEC TS 62758:2012. The HVDC source applied to the sample at $t = 0^+$to the samples to estimate the charge injection in the sample. A single-step voltage was applied to the sample along with a probing pulse of 600 V and pulse width of 3 ns and space charge was measured for up to 3600 seconds under 20 kV/mm (low field) and 80 kV/mm (high field). The pulse source is the series-connected coupling capacitor which prevents any incoming current from the HVDC source; even under breakdown. The experiments were conducted at a constant ambient temperature of 25℃. A total of 115 samples were tested. The safety resistor limits the current if any breakdown occurs during the measurement. The PVDF (Polyvinylidene fluoride) sensor is used to measure the output signal; it is amplified and measured in the oscilloscope. The entire test setup was placed in the oven to maintain a controlled temperature.

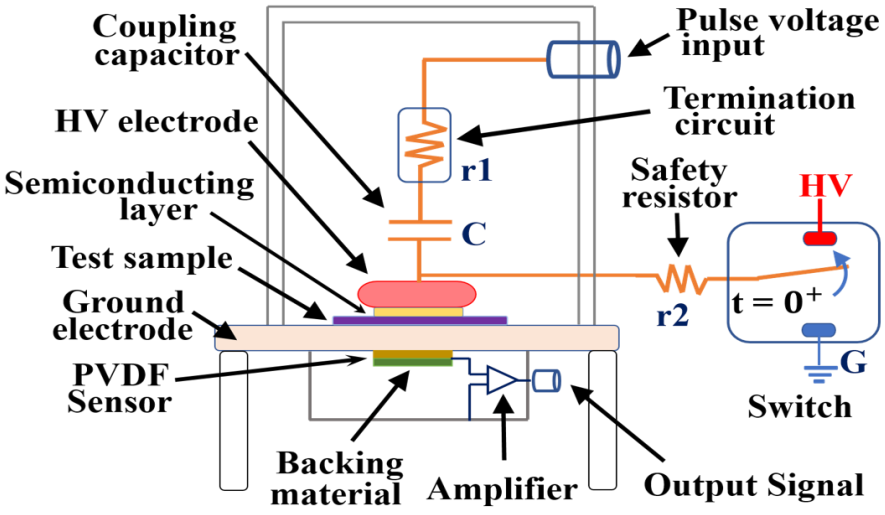

Fig.4. 2. PEA space charge measurement setup.

4.3. Results and Discussion

In this section, the various results are presented. The formation of space charge was examined for fresh and aged samples under low and high electric fields. In addition, the net charge in the insulation bulk and field enhancement factor (FEF) were calculated and plotted for each measurement. The FEF is calculated using the following equation:

$$FEF = \frac{E_{max} - E_{avg}}{E_{avg}} \times 100\% \qquad (4.1)$$

where, E_{max}= Maximum Electric Field (kV/mm) and E_{avg}= Average Electric Field (kV/mm).

The net charge density in the insulation bulk, until the breakdown, was calculated using

$$Net\ Charge = \frac{1}{d}\int_{0+}^{d-} |Q_1 - Q_t|.dx \tag{4.2}$$

where, Q_1 denotes the space charge density (C/m^3) at first time instant and Q_t is charge density (C/m^3) at any given time instant t, while d is the sample thickness (m).

The net charge density in the insulation bulk after breakdown can be calculated using

$$Net\ Charge = \frac{1}{d}\int_{0+}^{d-} |Q_{at}|.dx \tag{4.3}$$

where: Q_{at} is the space charge density (C/m^3) after breakdown

Further, the effect of ageing temperature and ageing duration on space charge dynamics in thermally aged LDPE samples was investigated. Also, the space charge profile was experimentally measured up to breakdown in highly aged samples and net charge and FEF were estimated. The results are followed by a detailed discussion and interesting inferences are drawn.

4.3.1 Space Charge Dynamics at Low Electric Field

The space charge and corresponding electric field plots at low field (20 kV/mm) for fresh and 80℃ aged samples, aged for different durations are shown in Fig. 4.3. It is observed that there is negligible charge injection as well as field enhancement in case of fresh samples at low electric field, as seen in Figs. 4.3 (a), (b), Fig. 4.4 and Fig. 4.5. The homocharge profile was observed in case of low aged samples (32, 64 days), as seen in Figs. 4.3 (c), (e). For higher aged samples (128, 256 days), homocharge is observed initially, however, after certain time, there is a transition in space charge regime from homo to heterocharge, as seen in Figs. 4.2 (g), (i).

The net charge in the bulk and FEF for fresh and aged samples (80℃) are plotted in Fig.4.4 and Fig. 4.5 respectively. It is observed that, towards the end of measurement duration (i.e. 1 hour), the magnitude of injected charge increased slightly in aged samples and thus net charge and FEF are relatively higher compared to fresh samples. Among aged samples, there is not much significant variation in net charge beyond ageing duration of 64 days as shown in Fig. 4.5, however, FEF tends to increase with ageing duration, as shown in Fig.4. 5.

The comparison of net charge in the bulk and FEF for fresh samples and 70℃ aged samples is shown in Fig.4.6 and Fig. 4.7 respectively. In this case, among aged samples, both net charge and FEF are almost invariant beyond ageing of 64 days, towards the end of measurement duration. Since the variation in the space charge and electric field profile for 70℃ aged samples under low field is not that much notable when compared to 80℃ aged samples, the corresponding plots are not shown here.

Fresh sample

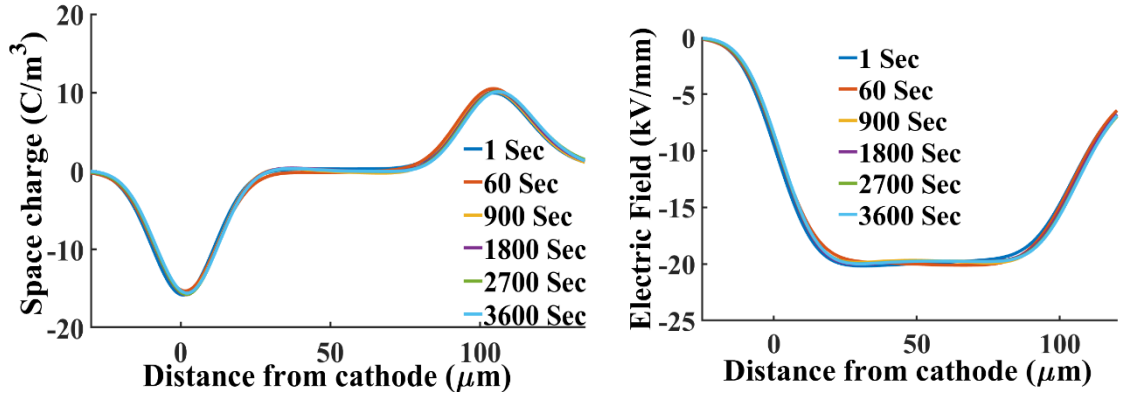

(a) **(b)**

32 days aged

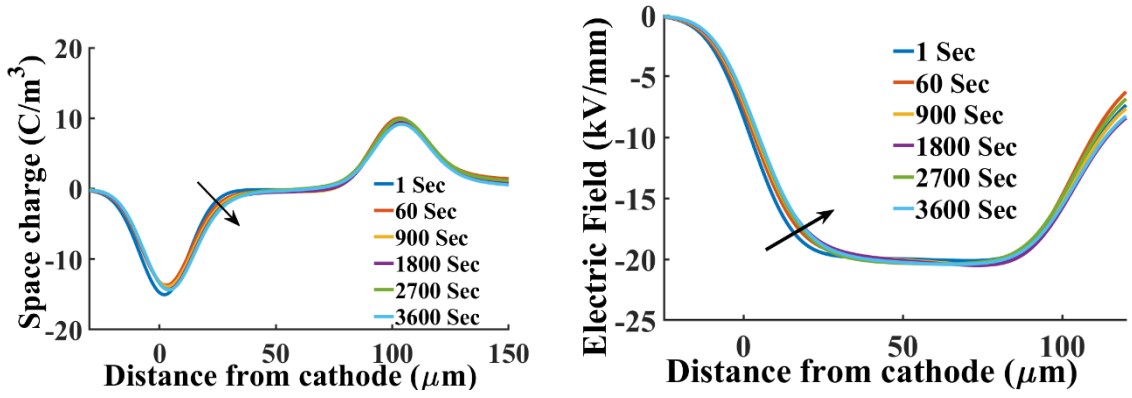

(c) **(d)**

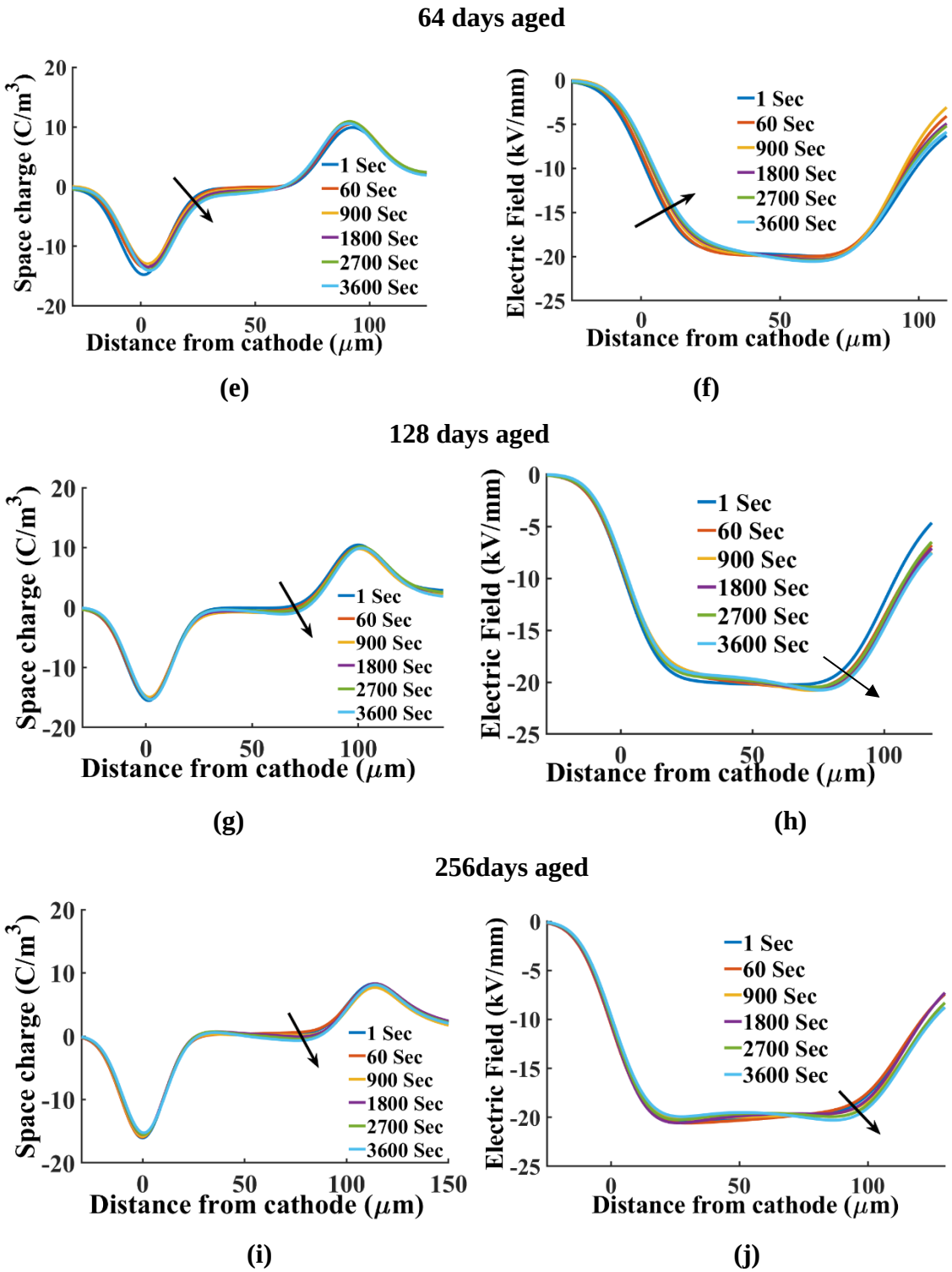

Fig. 4.3. Space measurement at low electric fields ($20kV/mm$). The space charge plot for fresh samples, 32, 64, 128, 256 days aged at 80℃ samples is (a) (c), (e), (g) and (i), and corresponding electric field plots is (b), (d), (f), (h) and (j).

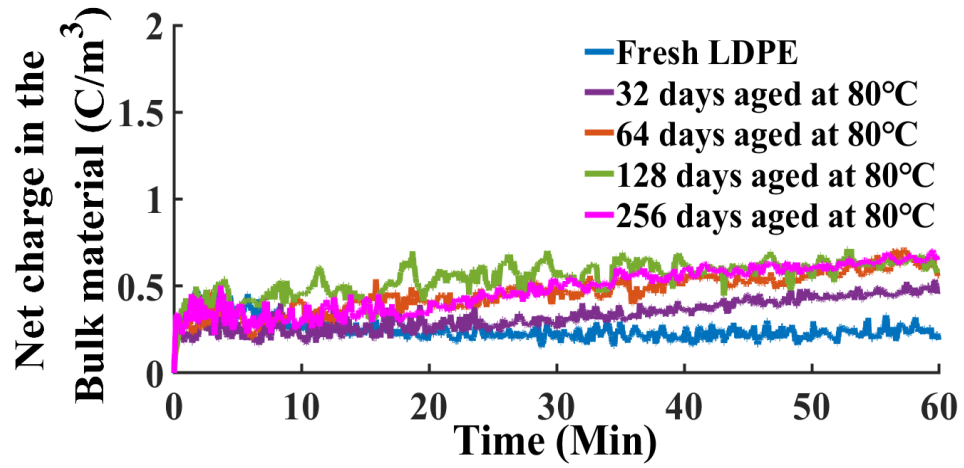

Fig. 4.4. Comparison of net charge in insulation bulk material of 80℃ aged samples with fresh sample, measured at 20 kV/mm

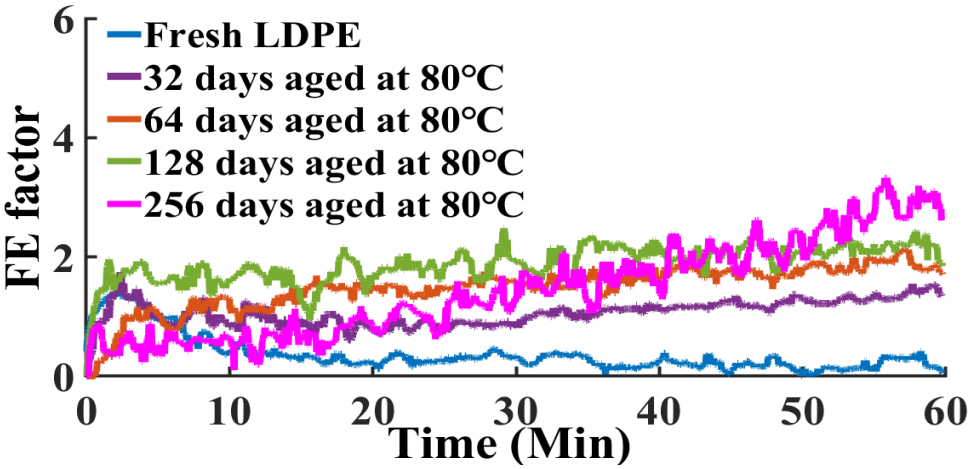

Fig. 4.5. Comparison of FEF in insulation bulk material of 80℃ aged samples with fresh sample, measured at 20 kV/mm

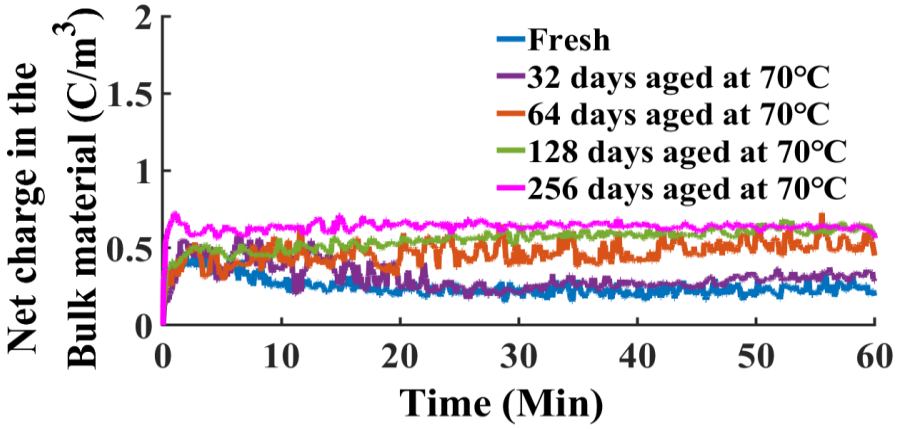

Fig. 4.6. Comparison of net charge in insulation bulk material of 70℃ aged samples with fresh sample, measured at 20 kV/mm.

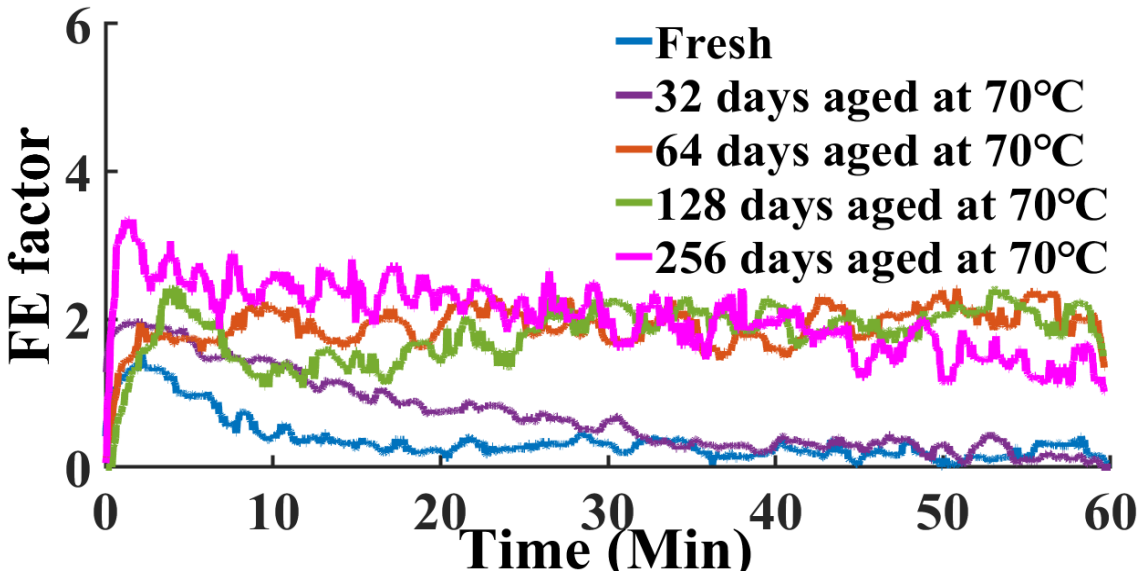

Fig. 4.7. Comparison of FEF in insulation bulk material of 70℃ aged samples with fresh sample, measured at 20 kV/mm.

4.3.2 Space Charge at High Electric Field

In this sub-section, the formation and effect of space charge under high electric field (80 kV/mm) have been investigated with respect to ageing temperature and duration. The space charge and electric field plots of samples aged at 70℃ for different durations are shown in Fig. 4.8. In fresh samples, clear hetero charge formation is observed (Fig. 4.8 (a)), as also reported in [40]. However, homocharges are present in case of aged samples (aged upto 128 days), as seen in Figs. 4.8 (c), (e) and (g).

The net charge and FEF for fresh and 70℃ aged samples are shown in Fig.4.9 and Fig.10 respectively. Up to the ageing duration of 128 days, the net charge at the end of measurement duration, increases with ageing period, however, the magnitude is relatively low, compared to that for fresh samples, as shown in Fig. 4.9. This may be attributed to the concentration of high amount of heterocharge in a smaller region in fresh samples, leading to higher field enhancement, as inferred from Figs. 4.8 (a) and (b), which in contrast with aged samples exhibit homocharge formation of relatively lower magnitude. The FEF also almost follows the same trend as net charge, as shown in Fig. 4.10.

Fresh sample

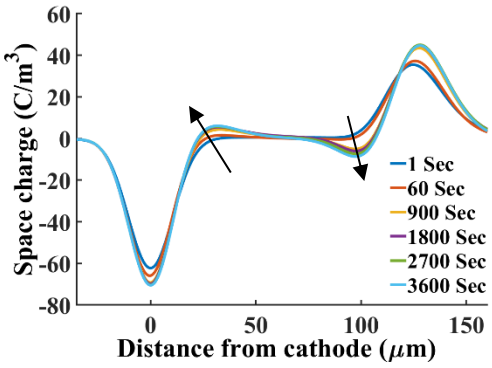

(a)

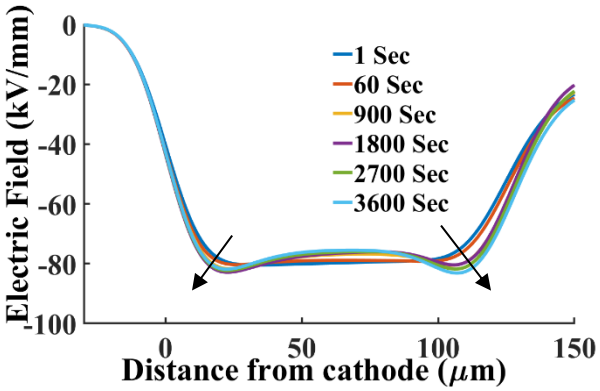

(b)

32 days aged

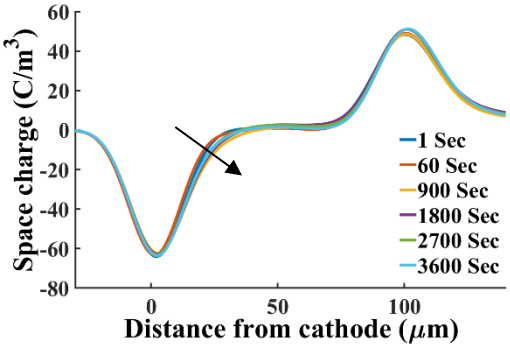

(c)

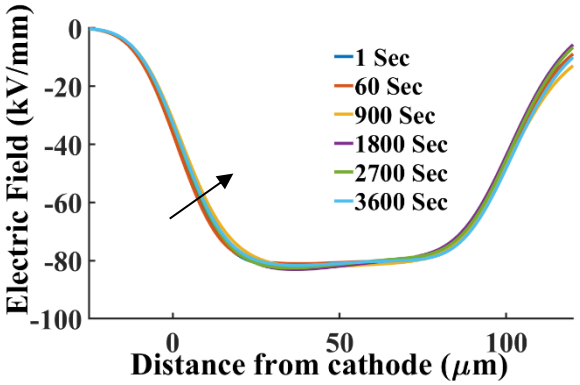

(d)

64 days aged

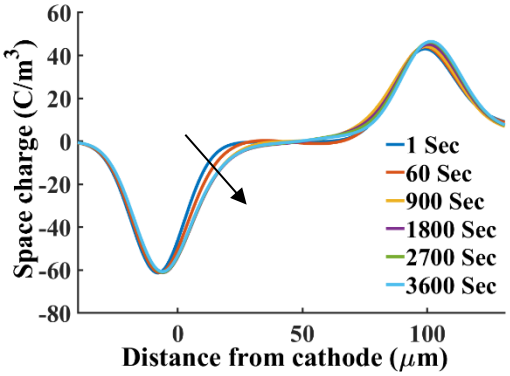

(e)

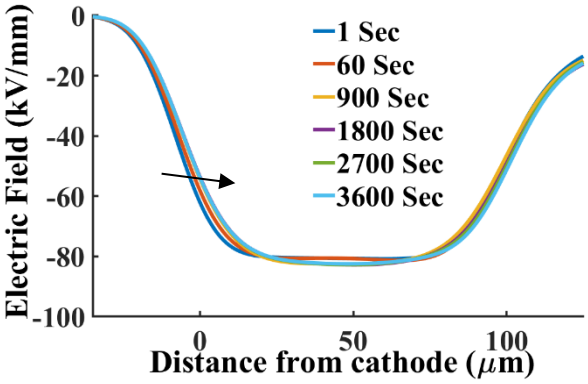

(f)

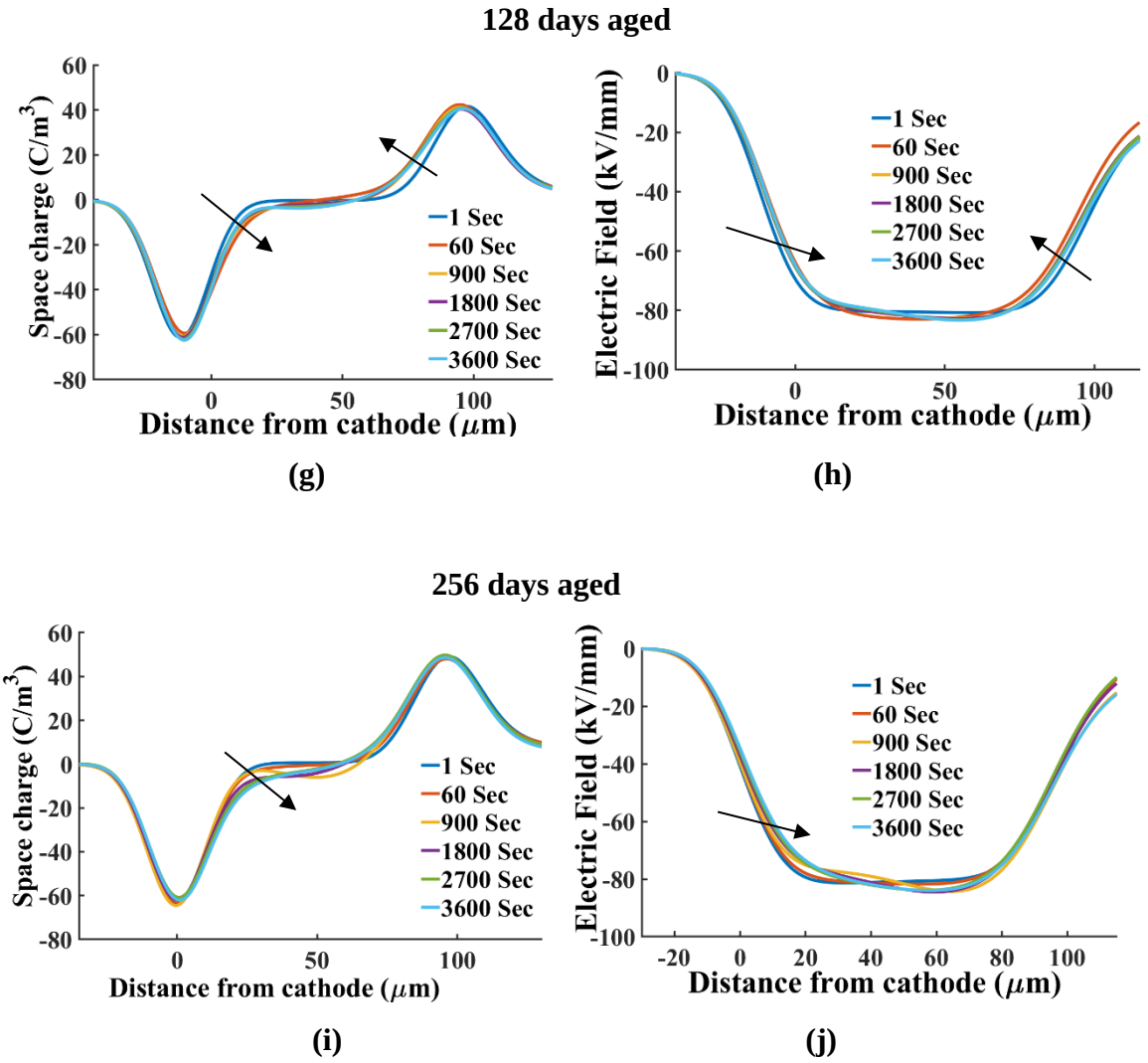

Fig. 4.8. Space measurement at high electric fields 80 kV/mm. The space charge plot 32, 64, 128, 256 days aged at 70℃ samples is (a) (c), (e), (g) and (i), and corresponding electric field plots is (b), (d), (f), (h) and (j).

In long-term aged (256 days) aged samples, initially homo charges are observed, as seen in Fig. 4.8 (i). However, with time, a packet like charge movement (particularly negative charge) towards the anode is observed. For a certain time period (10 min to 20 min), there is negligible charge injection (Fig. 4.9), but beyond that a high amount of negative charge is injected from the cathode, which further contributes to the packet charge movement, as discussed in later section (Fig. 4.20). The FEF was also found to be highest compared to all other samples, as seen in Fig. 4.10. In case of 256 days aged samples (70℃), however, breakdown was not observed up to the end of measurement duration.

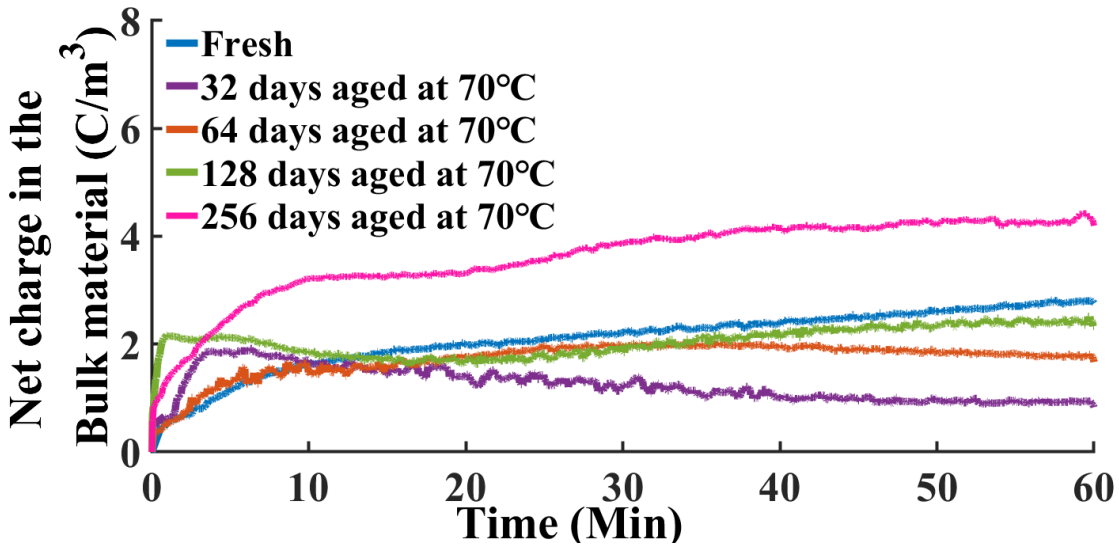

Fig. 4.9. Comparison of net charge in insulation bulk material of 70°C aged samples with fresh sample, measured at 80 kV/mm.

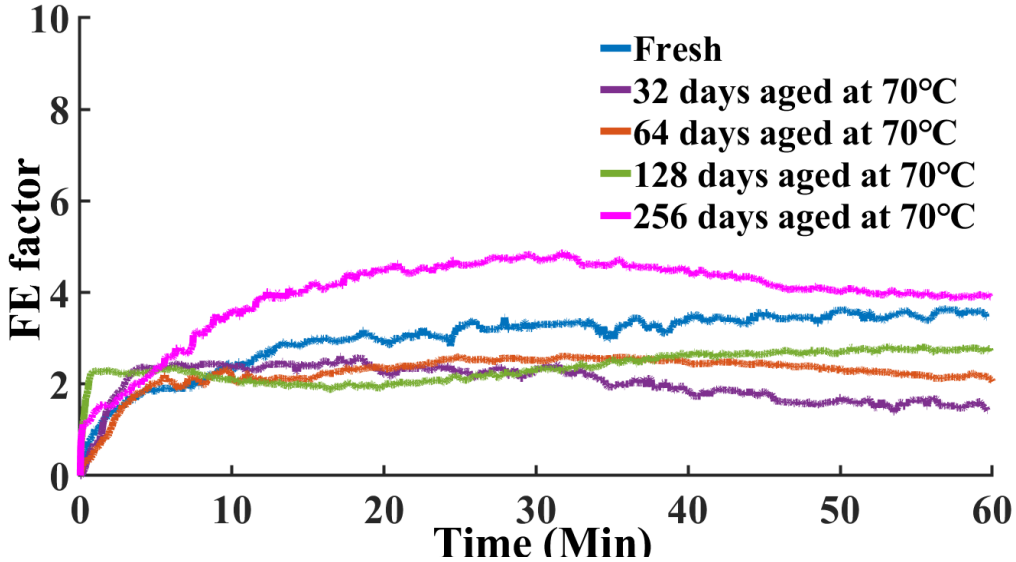

Fig. 4.10. Comparison of FEF in insulation bulk material of 70°C aged samples with fresh sample, measured at 80 kV/mm.

The space charge and electric field plots for samples aged at 80°C are shown in Fig. 4.11, while the net charge and FEF are shown in Fig. 4.12 and Fig. 4.13 respectively. A clear homocharge profile was observed for samples aged up to 64 days. In case of 32 days aged samples, the charges are injected from both electrodes, leading to homocharge formation as seen in Fig. 4.11 (a) and beyond a certain time (~10 min), the injectedcharge tends to saturate, as seen in Fig. 4.12.

The 64 aged samples exhibited a peculiar behaviour. The injection of charges causes homocharge as in Fig. 4.11 (c) and there is an increase in the net charge magnitude up to about 7 min, but beyond that, the net charge in the bulk tends to reduce as seen in Fig. 4.12. The decrease in the net charge in the bulk is accompanied by a simultaneous increase in the cathode peak, as may be inferred through the space charge plot at the 900th and 1800th second in Fig. 4.11 (c). However, towards the end of measurement duration, the net charge again tends to increase, as in Fig. 4.12.

In case of 128 days aged samples, the injection of charge happens in the entire bulk material, leading to a packet like charge formation, which moves through the bulk towards the other electrode as discussed in the later section (Fig 4.20). For all the samples, the FEF was observed to follow almost the similar trend as that of the net charge, as shown in Fig. 4.13.

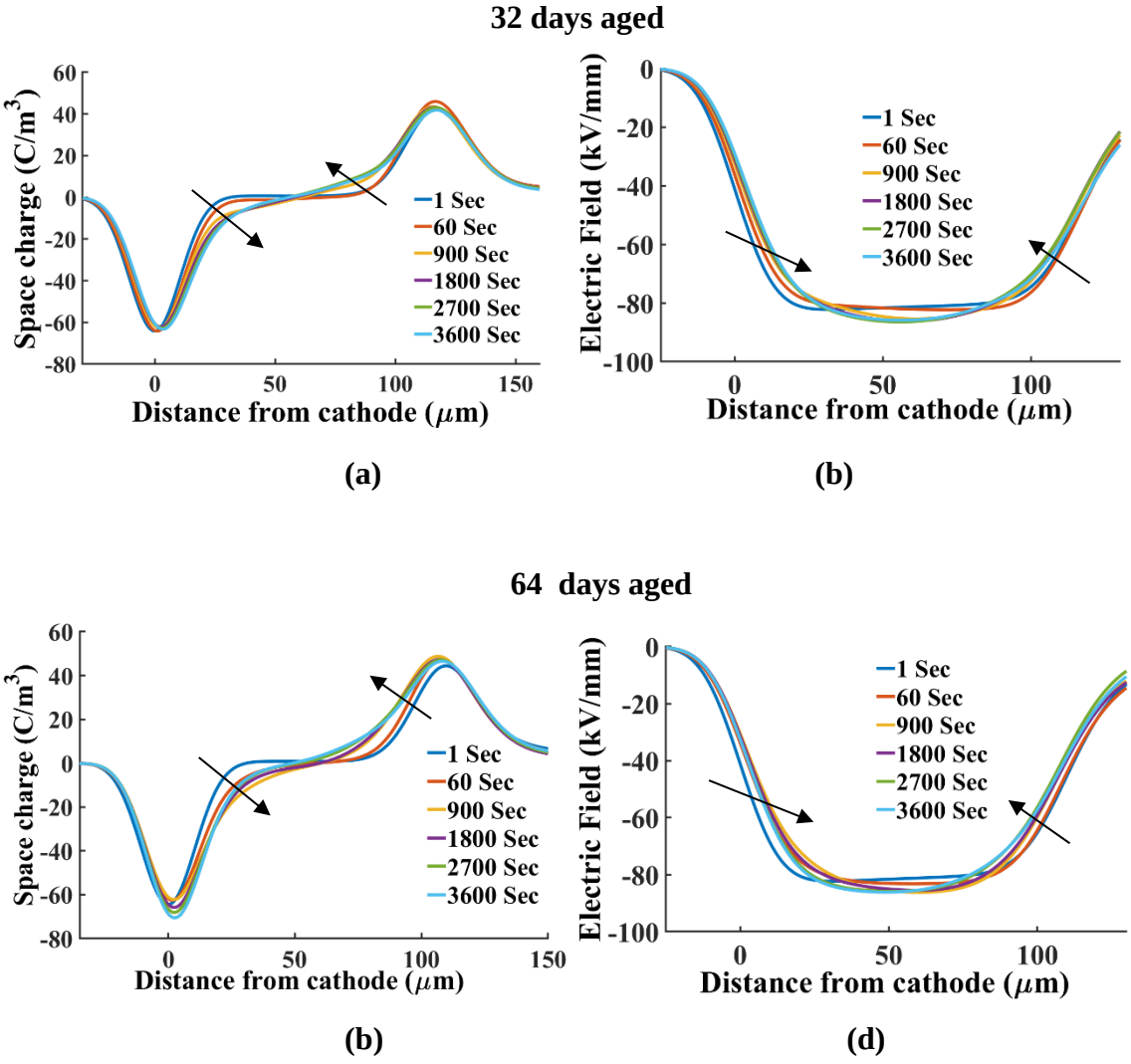

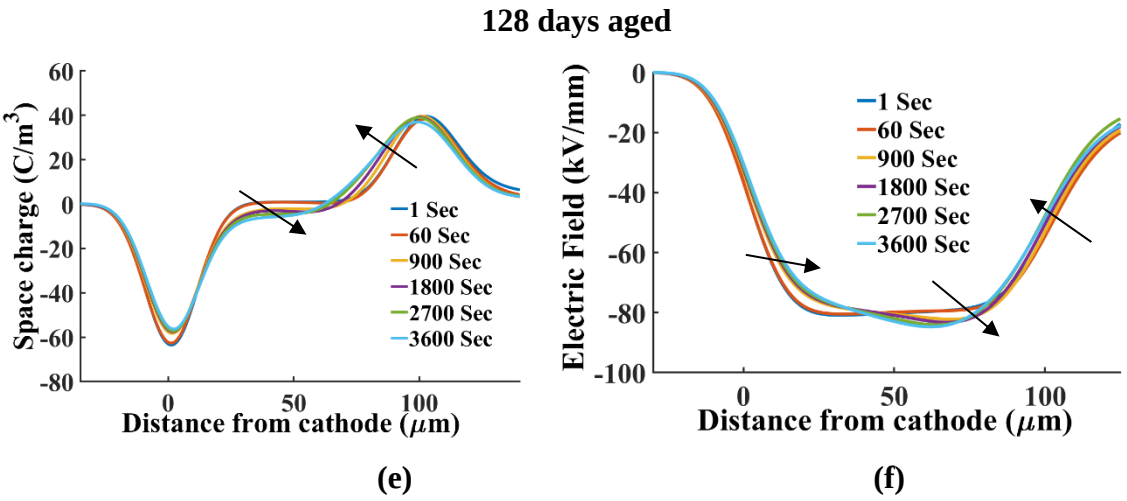

Fig.4.11. Space measurement at high electric fields $80kV/mm$. The space charge plot for fresh samples, 32, 64, 128 aged at 80℃ samples is (a) (c), (e) and (g), the corresponding electric field plots is (b), (d), (f) and (h).

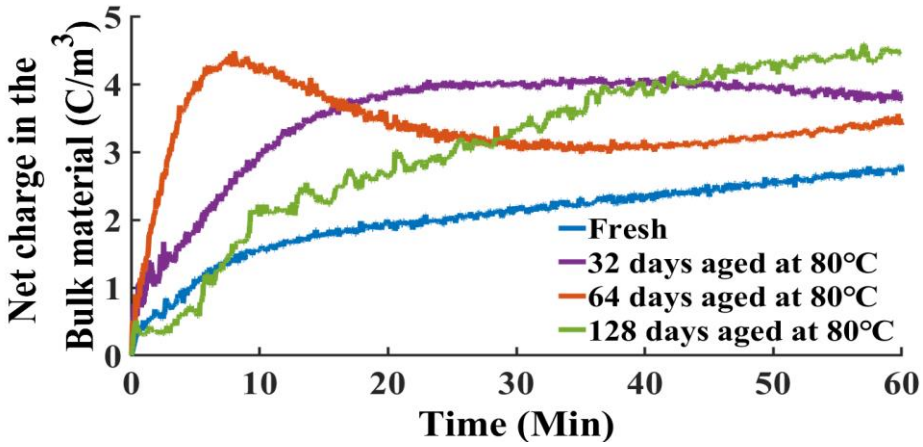

Fig. 4.12. Comparison of net charge in insulation bulk material of 80℃ aged samples with fresh sample, measured at 80 kV/mm.

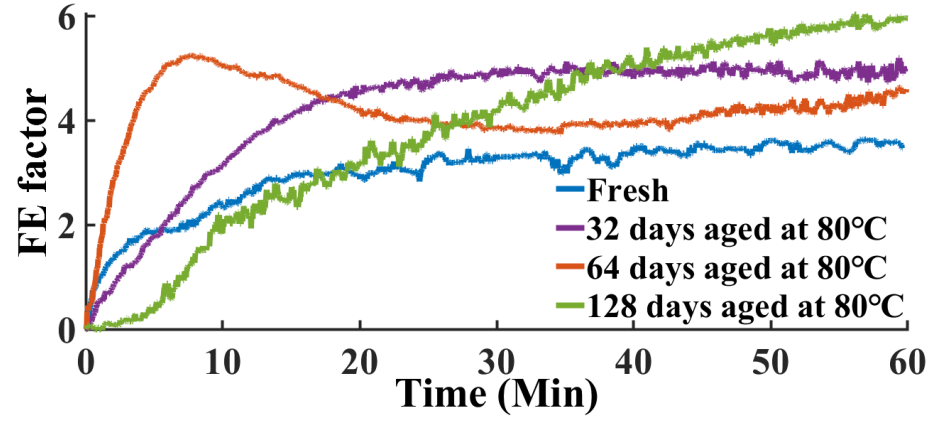

Fig. 4.13. Comparison of FEF of 80℃ aged samples with fresh sample, measured at 80 kV/mm.

4.3.3 Space Charge Dynamics until Breakdown

It is known that the breakdown mechanism of a dielectric under DC fields is closely related to the space charge formation [46], [47]. Therefore, estimation of space charge near breakdown assumes great significance. In the erstwhile works, a positive packet like charge movement was reported, just before breakdown in virgin LDPE films [46-48], however, space charge dynamics until breakdown have not been reported for long-term, highly aged LDPE samples, until now. In this sub-section, the author presents interesting insights on space charge phenomenon till breakdown at 80 kV/mm for 256 days aged samples (80℃). The series of events relating space charge and associated breakdown may be summarized in four stages:

Stage 1: Initially (i. e. up to few seconds), injection of charge was observed from both anode and cathode and thus the space charge assumes a homocharge profile. However, shortly thereafter (typically 40 seconds), a high amount of negative charge injection was observed up to ∼10 min, leading to a packet-like charge movement in the bulk material towards the anode. The injection from anode was found to be negligible compared to the injection from cathode. The packet charge movement is associated with a reduction in the cathode peak, whereas the anode peak is relatively invariant as shown in Fig. 4.14 and Fig. 4.18.

Stage 2: After about 10 min, there was a saturation in the number of injected charges for upto 5 min, however even during this duration, the negative packet-type charge movement was observed in the bulk as shown in Fig. 4.19 (f).

Stage 3: Beyond 15 min (i.e., after saturation or holding time), injection resumed, with a very amount of negative charge injection from cathode. Just before the breakdown, the bulk material was almost fully filled with negative charges. The field enhancement occurs near the anode due to the movement of negative packet charge, which leads to concentration of electric field in a small region near the anode, which tends to initiate breakdown, as shown in Fig. 4.15 and Fig. 4.19 (f). The breakdown was found to occur immediately after the 2585^{th} second. The net charge just before breakdown was found to increase to a very high value (Fig. 4.16). The field enhancement factor until the breakdown is shown in Fig.4. 17. Just before the breakdown, the FEF reaches to ∼12%.

Stage 4: Just after the breakdown, it was observed that the charge density on the electrodes tends to reverse in polarity, as shown in Fig. 4.14 and Fig. 4.18. However, inside the insulation bulk, the accumulated charge has the same polarity as that before breakdown, though with less magnitude, which may be due to some recombinations occurring within the breakdown channel. Due to this, the net charge in the bulk of insulation material tends to reduce post breakdown, as shown in Fig. 4.16.

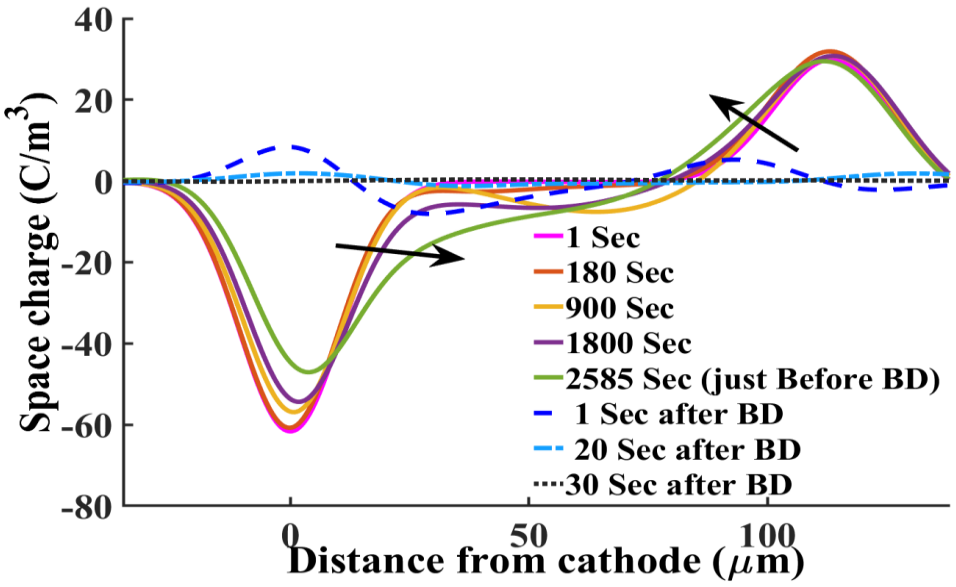

Fig. 4.14. Space charge at different time instants from initial to until breakdown and after breakdown.

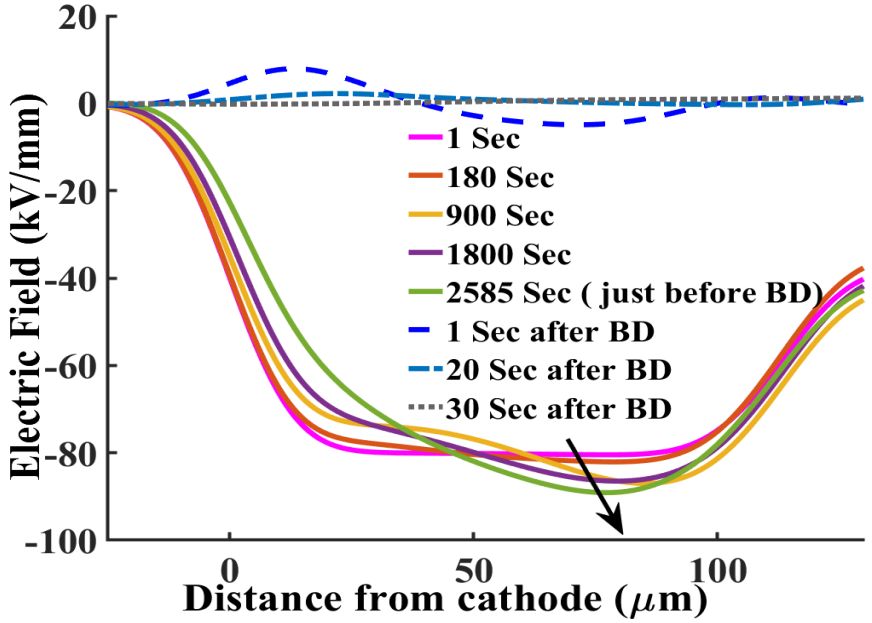

Fig. 4.15. Electric Field at different time instants from initial to until breakdown and after breakdown.

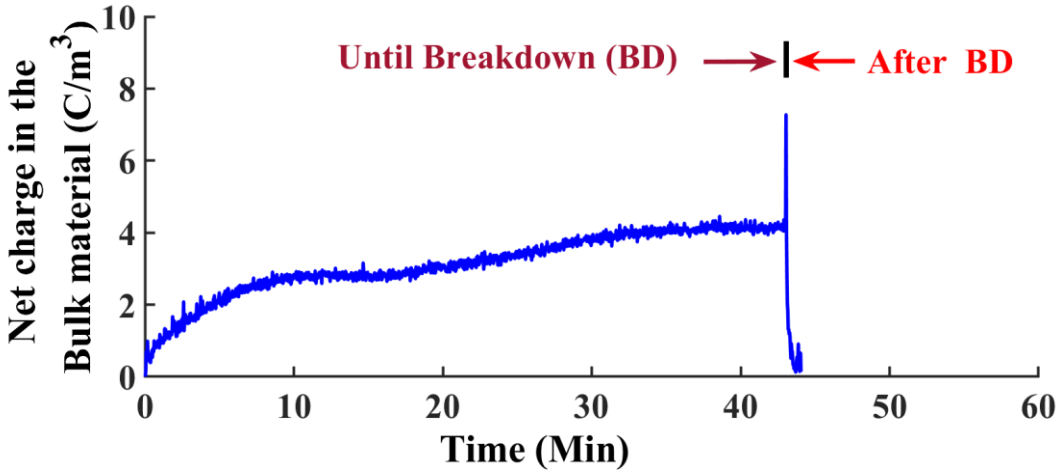

Fig. 4.16. Net charge until breakdown and after the breakdown.

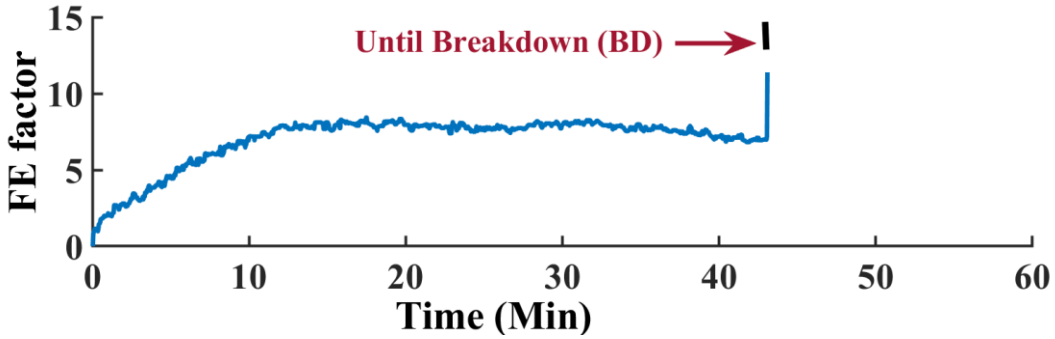

Fig. 4.17. Field enhancement factor until breakdown.

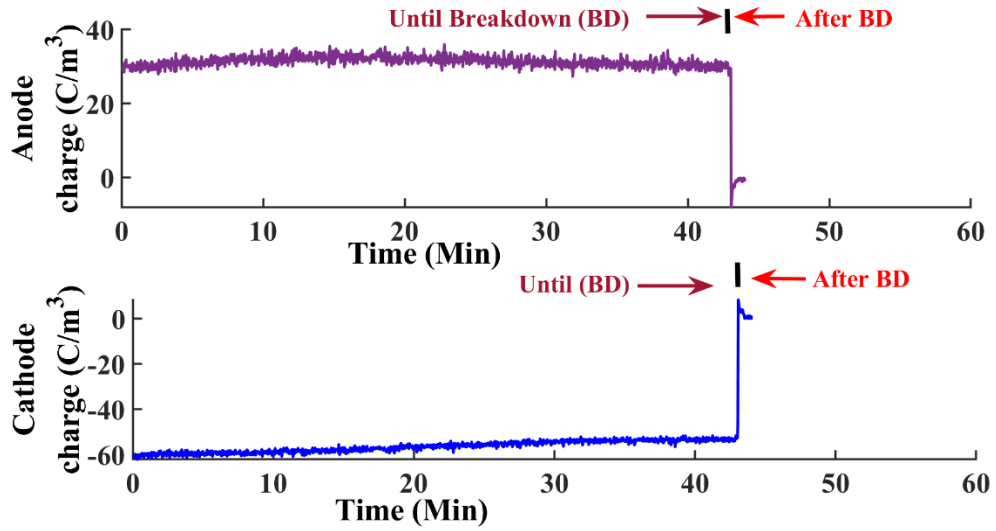

Fig. 4.18. Anode and cathode charges at the time of breakdown.

The inter-related space charge and breakdown mechanism may be explained physically as follows. If we consider the insulation material to be consisting of multiple parallel resistors, as shown in Fig. 4.19 (a), then, irrespective of the breakdown initiating from either anode or cathode, one of the resistor would get short-circuited (R_X), and thus

$$R_1, R_2, \ldots R_{(n+1)} >>> R_X \tag{4.4}$$

where, R_X denotes the resistance of the short-circuited resistor, and $R_1, R_2, \ldots R_{(n+1)}$ denote the resistances of the healthy part of the insulation bulk.

In this case, the propagation of breakdown starts from near the anode, because of the high negative packet charge migration in the bulk material towards the anode. Thus, through this short-circuited (low resistive) path, the charges present on the anode and cathode surface tend to re-combine and neutralize. The accumulated space charges in the insulation bulk near that channel also tend to recombine through the channel and vanish.

However, the space charges which are away from this channel are still present because of the very high resistance path in the remainder of the bulk. In order to neutralize the average electric field produced by these accumulated charges, opposite charges are injected into both electrodes from the ground through the conducting channel, as inferred from Fig. 4.14 and Fig.4.19 (d). The opposite charges on the electrode are present for some time and decay eventually. After some seconds, the charges in the insulation material also decay, this occurs in approximately 30 seconds.

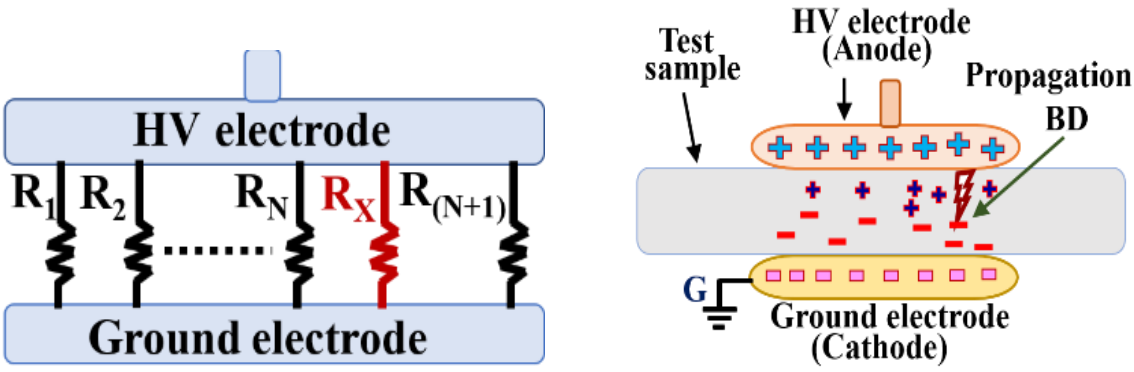

(a) **(b)**

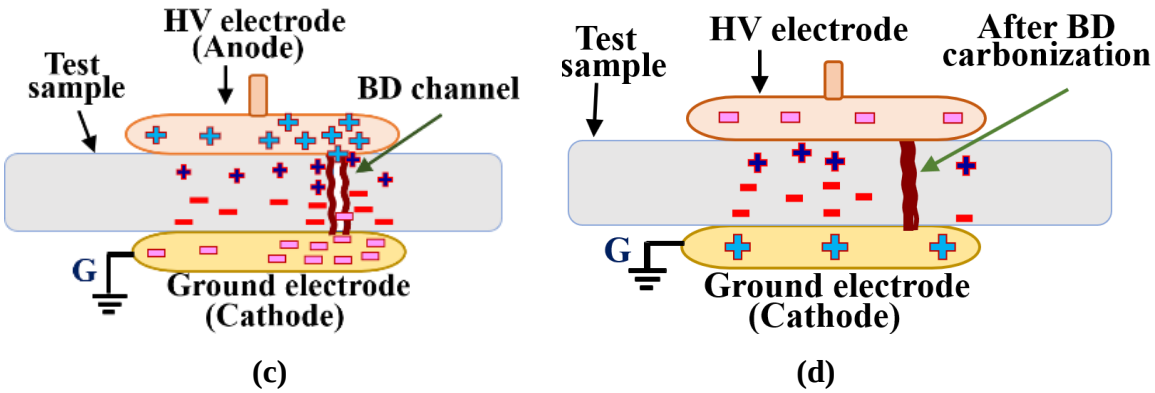

Fig. 4.19. Schematic diagram of flow of charge during/after breakdown (a to d).

4.3.4 A Brief Summary of Investigations

In this sub-section, for a better visual understanding of the results, an overview is presented in terms of 2D colour maps, which give a clear view of charge injection and charge movement through the bulk.

Fig. 4.20 (a) and (b) present a comparison of space charge profile with varying applied field in fresh samples. As discussed before, negligible injection was seen at low field whereas a clear heterocharge profile was observed under high field.

In Fig. 4.20 (c), (d) and (e), a comparison is made of charge profile under high field, with respect to the ageing duration, for samples aged at 80℃. Homocharge profile was observed with an increase in the charge injection with ageing duration. For 128 days aged samples, a packet-like charge movement was seen.

Space charge dynamics for long-term aged (256 days aged) samples under high field are compared with respect to the ageing temperature in Fig. 4.20 (f) and (g). For both ageing temperatures i.e., 70℃ and 80℃, a negative, packet-like charge was seen. However, in case of the latter, breakdown occurred in the samples, which is attributed to the high amount of negative packet charge movement towards anode through the bulk. This observation is in contrast to the findings of [47], where for fresh LDPE samples, breakdown was preceded by a positive packet-like charge formation and movement. Also, it was observed that an FEF of 11.4% is sufficient to initiate breakdown, unlike in [47] where very high values of FEF are reported for fresh samples, just before breakdown.

Fresh LDPE (20 kV/mm)

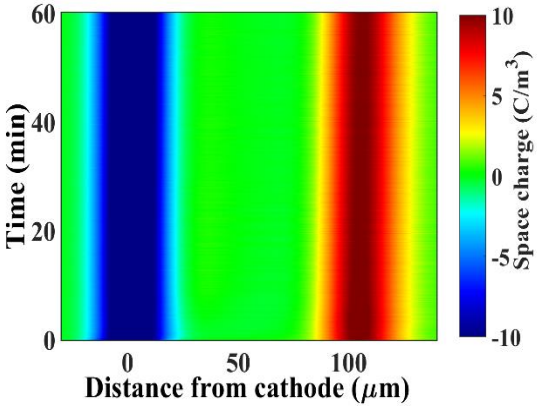

(a)

Fresh LDPE (80 kV/mm)

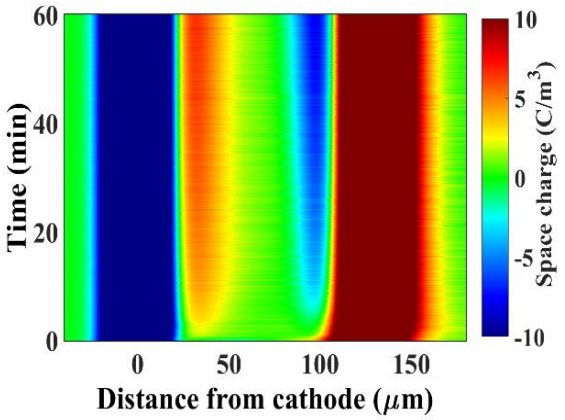

(b)

32 days aged at 80℃ (80 kV/mm)

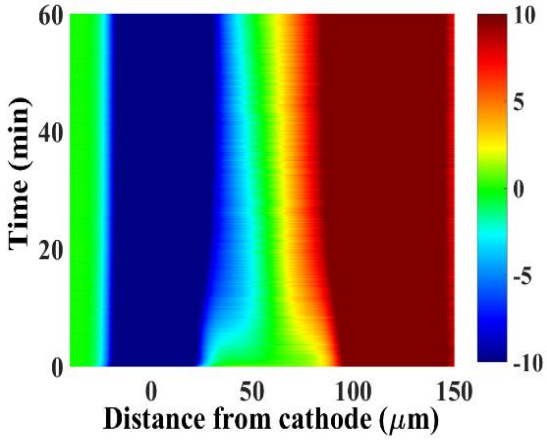

(c)

64 days aged at 80℃ (80 kV/mm)

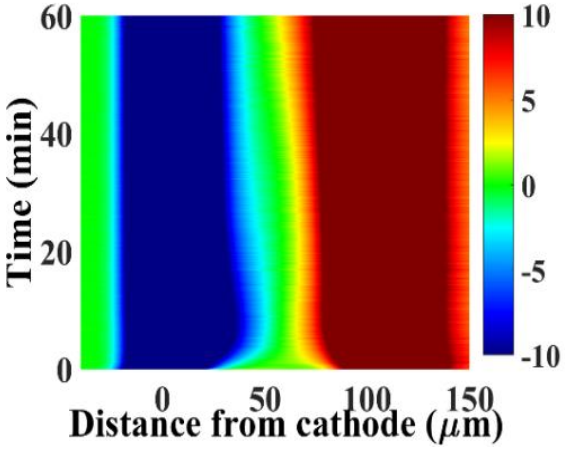

(d)

128 days aged at 80℃ (80 kV/mm)

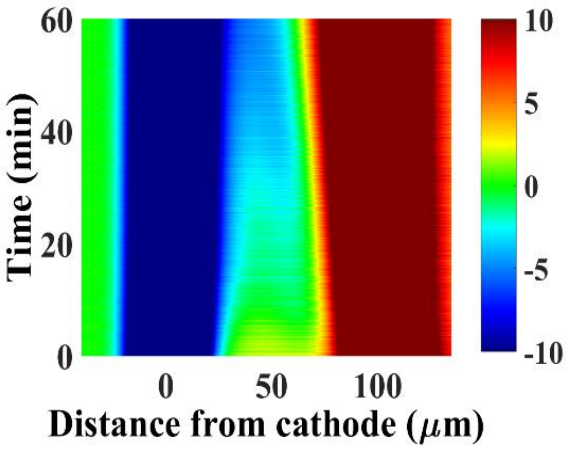

(e)

256 days aged at 80℃ (80 kV/mm)

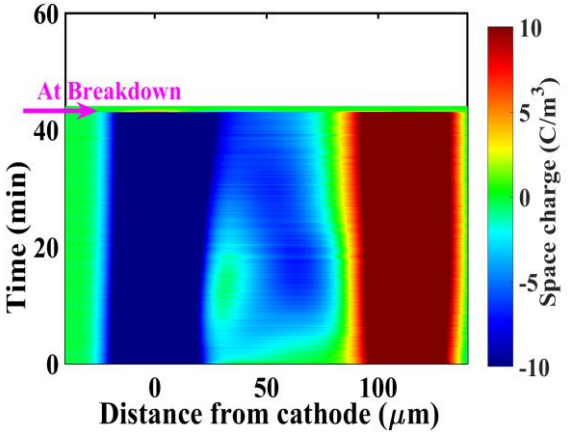

(f)

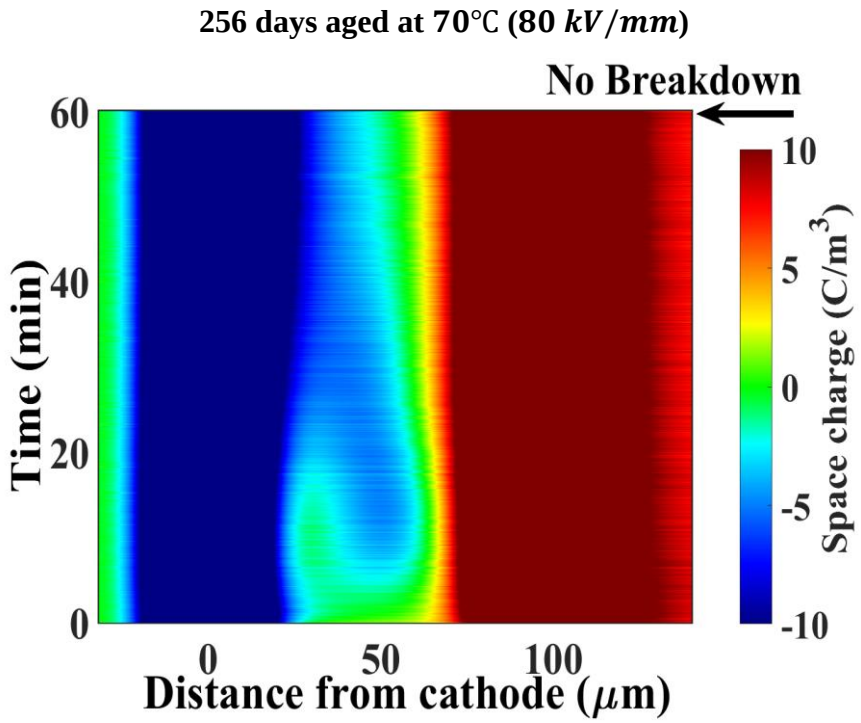

(g)

Fig.4. 20. Color map of space charge (a) fresh samples measures at 20kV/mm, (b) Fresh samples measured at 80kV/mm, (c) 32 days aged at 80℃ measured 80kV/mm (c) 64 days aged at 80℃ measured 80kV/mm (d) 128 days aged at 80℃ measured 80kV/mm (f) 256 days aged at 80℃ measured 80kV/mm clear view of packet charge movement until breakdown. (g) 256 days aged at 70℃ measured 80kV/mm (breakdown not occurred).

CHAPTER 5

Conclusions and Future Scope of the Work

5.1 Conclusions

Complete understanding of physical phenomena underlying electrothermal breakdown is essential for optimal design of power cable. Better design in turn contributes to higher lifetime, fewer failures, higher reliability of cable transmission network and hence power system. The author believes that the electro-thermal simulation model and experimental setup for breakdown of loaded HVDC cable, proposed in the first part of this thesis would contribute towards enhancement of existing knowledge and at the same time, would help the design engineers and power utilities. The second part of this thesis attempted to investigate the thermal aspects of space charge dynamics of a HVDC cable, which always tends to undergo ageing in field. The wide-known notion that space charge may lead to breakdown is experimentally investigated for highly aged samples and it is believed that the presented results and inferences would enable better understanding of the space charge phenomenon in HVDC cables. In conclusion the thesis contributes the following:

5.1.1 Simulation of Electro-thermal Runaway and Thermal Limits of a Loaded HVDC Cable

1. The main reason for breakdown in HVDC cables is the internal cascading in the insulation (i.e. intrinsic instability), however, the interaction of the cable with the outside environment (which has a finite thermal conductivity) will speed up the breakdown process (i.e. interactive instability).
2. The thermal conductivity of soil determines the rate of heat dissipation from the cable. For a soil having a poor (lower) thermal conductivity, the heat produced in the soil takes longer to dissipate, which causes accumulation of heat in cable, which may ultimately lead to the breakdown.
3. The back-fill (or soil) surrounding the cable assumes huge significance; even a short length of low thermal conductivity soil would trigger interactive thermal breakdown and leads to a drastic reduction in the breakdown voltage.

4. In case of transient breakdown of a loaded cable (i.e. when breakdown occurs before temperature stabilization), there is no effect of load variation. However, in case of steady-state breakdown (i.e. breakdown occurring after temperature stabilization), increase in load leads to a considerable reduction in the time to breakdown at a given voltage.
5. The loaded cable has less breakdown voltage than the cable under no-load conditions by a few 100's of kV.

5.1.2 Effect of Long-term Thermal Ageing on Space Charge Dynamics in LDPE

1. Under low electric fields (~20 kV/mm), negligible charge injection as well as field enhancement was observed in fresh samples. However, in low aged samples, homocharge profile was observed. For long-term aged samples (128 days and beyond), a transition was seen from initial homocharge to heterocharge regime towards the end of measurement duration (1 hour). The effect of ageing temperature is relatively less significant for low aged samples.
2. Under high fields (~80 kV/mm), a heterocharge profile was observed in fresh samples. In low aged samples, homocharge was observed, however, in long-term aged samples (128 days and beyond), a clear packet-like charge formation and movement was observed. Increase in ageing temperature causes increase in negative packet charge magnitude in long-term aged samples, however positive charge injection is relatively less in magnitude.
3. The FEF is observed to be following the net charge trend, however it is dependent on the distribution of charge in the bulk material as to whether it is equally distributed or only distributed in a particular region.
4. The breakdown in long-term and highly aged samples (80°C for 256 days) is preceded by a very high amount of negative packet-like charge movement towards anode, leading to initiation of breakdown in a small region near anode. Also, it was observed that an FEF of 11.4% is sufficient to initiate breakdown.

5.2 Future Scope of the Work

Based on the work presented in the thesis, some of the suggestions for the further work in near future, are the following:

1. There is scope for detailed investigations of the space charge dynamics until breakdown in multilayer dielectrics.
2. Electro-thermal model and experimental setup for lightning/switching impulse breakdown on cable insulation.
3. Investigation and modelling of chopped impulse breakdown of insulation.
4. The space charge until breakdown experiment can be conducted under electro-thermal stress.
5. The circuit model can be extended to multi-layer breakdown.

The author and his research supervisor are currently working on the above topics.

List of Publications

I. IEEE Transactions

1. **S. Dhayalan** and C. C. Reddy, "Simulation of Electro-Thermal Runaway and Thermal Limits of a Loaded HVDC Cable," in *IEEE Transactions on Power Delivery*, vol. 37, no. 4, pp. 2621-2628, Aug. 2022, doi: 10.1109/TPWRD.2021.3112558.

2. **S. Dhayalan and** C. C. Reddy, "Effect of Thermal Aging on Space Charge Dynamics in LDPE," in *IEEE Transactions on Dielectrics and Electrical Insulation*, vol. 30, no. 4, pp. 1725-1732, Aug. 2023, doi: 10.1109/TDEI.2023.3280147.

3. **S. Dhayalan** and C. C. Reddy, "Conduction and Breakdown Phenomena with Ageing of Low-Density Polyethylene" in *IEEE Transactions on Dielectrics and Electrical Insulation* (Under Preparation).

II. Patent

1. **Sathyamoorthy Dhayalan** and C. C. Reddy, "System and method for determining breakdown voltage of High Voltage Direct Current (HVDC) cable" **Indian Patent, no: 202111024296**, June 1, 2021.

III. IEEE International Conference Proceedings

1. **S. Dhayalan**, B. S. Thind and C. C. Reddy, "Transient Electric and Thermal Fields in a HVDC cable," 2021 *IEEE Conference on Electrical Insulation and Dielectric* Phenomena (CEIDP), 2021, pp. 187-190, doi: 10.1109/CEIDP50766.2021.9705374.

2. **D. Sathyamoorthy** and C. C. Reddy, "Experimental investigations on breakdown in cable insulation," 2017 *International Symposium on Electrical Insulating Materials (ISEIM)*, 2017, pp. 570-573, doi: 10.23919/ISEIM.2017.8166553.

3. **S. Dhayalan**, A. Das, P. Johri and C. C. Reddy, "Estimation of Electric Field and Temperature in HVDC Cables Under Different Environmental Conditions," 2021

IEEE 16th International Conference on Industrial and Information Systems (ICIIS), 2021, pp. 262-264, doi: 10.1109/ICIIS53135.2021.9660725.

4. **S. Dhayalan**, A. H. Kumar, P. Johri and C. C. Reddy, "Electro-thermal Dynamics During Load Cycle and Polarity Reversal of HVDC Cables Under Different Soil Conditions," 2021 *International Conference on Electrical, Computer and Energy Technologies (ICECET)*, 2021, pp. 1-4, doi: 10.1109/ICECET52533.2021.9698421.

5. **D. Sathyamoorthy** and C. C. Reddy, "An Attempt to Estimate DC Endurance Coefficient from Volume Resistivity," 2019 *IEEE 4th International Conference on Condition Assessment Techniques in Electrical Systems (CATCON)*, 2019, pp. 1-3, doi: 10.1109/CATCON47128.2019.CN0006.

6. **S. Dhayalan**, B. Das, P. Johri and C. C. Reddy, "Experiment and Simulation of Leakage Current in HVDC Cable under Different Electro-Thermal Stresses," 2021 *IEEE 5th International Conference on Condition Assessment Techniques in Electrical Systems (CATCON)*, 2021, pp. 335-338, doi: 10.1109/CATCON52335.2021.9670473.

IV. CIGRE International Conference Proceedings

1. **Sathyamoorthy Dhayalan**, Pranav Johri and C. C. Reddy, "Simulation and Experimental Investigation of Maximum Power Transfer Capability of HVDC Cables", Proceedings, *Jicable HVDC'21, International Symposium on HVDC Cable Systems-2021*, 29, Young Researchers' Contest, Liege, Belgium.

V. Awards

1. **Won 2nd Prize award in** Young Researchers' Contest in **Jicable HVDC'21** held in Liege, **Belgium,** on 9th Nov 2021, for the paper titled **"**Simulation and Experimental Investigation of Maximum Power Transfer Capability of HVDC Cables".

2. **Won Prize award** in **POSOCO Power System Awards (PPSA) in** December 2021, on the title of "Simulation and Experimental Investigations of Electro-Thermal Breakdown in Polymeric Cables".

3. Won **Prize award** in **INAE (Indian National Academy of Engineering)** 100s in December 2021, on the topic of "Experimental Determination of Exact Breakdown strength of High Voltage Cables".

References

[1]. T. L. Hanley, R. P. Burford, R. J. Fleming and K. W. Barber, "A general review of polymeric insulation for use in HVDC cables," in *IEEE Electrical Insulation Magazine*, vol. 19, no. 1, pp. 13-24, Jan.Feb. 2003.

[2]. V. Vahedy, "Polymer insulated high voltage cables," in *IEEE Electrical Insulation Magazine*, vol. 22, no. 3, pp. 13-18, May-June 2006.

[3]. W. T. Starr, "Polymeric outdoor insulation," in *IEEE Transactions on Electrical Insulation*, vol. 25, no. 1, pp. 125-136, Feb 1990.

[4]. K. Meah and S. Ula, "Comparative Evaluation of HVDC and HVAC Transmission Systems," *2007 IEEE Power Engineering Society General Meeting*, 2007, pp. 1-5, doi: 10.1109/PES.2007.385993.

[5]. Y. Zhou, S. Peng, J. Hu and J. He, "Polymeric insulation materials for HVDC cables: Development, challenges and future perspective," in *IEEE Transactions on Dielectrics and Electrical Insulation*, vol. 24, no. 3, pp. 1308-1318, June 2017, doi: 10.1109/TDEI.2017.006205.

[6]. S. Nishikawa, K.-I. Sasaki, K. Akita, M. Sakamaki and T. Kazama, and K. Suzuki, "XLPE cable for DC link", *Sei Tech. Rev.*, Apr. 2017, [online] Available: https://global-sei.com/technology/tr/bn84/pdf/84-10.pdf.

[7]. Chizuo Watanabe,Yasuo Itou,Hidetaka Sasaki,Yoshinao Murata,Makoto Suizu,Masatoshi Sakamaki,Masaru Watanabe,Shoshi Katakai, " Practical Application of ±250-kV DC-XLPE Cable for Hokkaido–Honshu HVDC Link", *Wiley Online Library.*, Jan. 2015, [online] Available: https://onlinelibrary.wiley.com/doi/abs/10.1002/eej.22706.

[8]. F. Meng, C. Dai, A. Paramane, X. Chen and Y. Tanaka, "Effect of Thermal Ageing on Insulation Properties of 500 kV DC XLPE Submarine Cable Insulation," 2020 IEEE Conference on Electrical Insulation and Dielectric Phenomena (CEIDP), 2020, pp. 516-519, doi: 10.1109/CEIDP49254.2020.9437442.

[9]. L. Boukezzi, A. Boubakeur, C. Laurent and M. Lallouani, "DSC Study of Artificial Thermal Aging of XLPE Insulation Cables," *2007 IEEE International Conference on Solid Dielectrics*, 2007, pp. 146-149, doi: 10.1109/ICSD.2007.4290774.

[10]. Y. Zhang, Y. Zhao, G. Yu, L. Chen, Y. Wang and L. Zheng, "Research of the key issues of ±535kV HVDC extruded cable development," 2020 4th International Conference on HVDC (HVDC), 2020, pp. 1139-1142, doi: 10.1109/HVDC50696.2020.9292776.

[11]. X. Qi, Z. Zheng and S. Boggs, "Engineering with nonlinear dielectrics," in *IEEE Electrical Insulation Magazine*, vol. 20, no. 6, pp. 27-34, Nov.Dec. 2004, doi: 10.1109/MEI.2004.1367508.

[12]. R. Coelho, "Charges in non homogeneous dielectrics," IEEE 1997 *Annual Report Conference on Electrical Insulation and Dielectric Phenomena*, 1997, pp. 1-10 vol.1, doi: 10.1109/CEIDP.1997.634546.

[13]. C. C. Reddy, "Field-Temperature aided conduction and breakdown in HVDC cables" ,. PhD Thesis 2008.

[14]. R. Bodega, "Space charge accumulation in polymeric high voltage DC cable systems",. PhD Thesis 2006.

[15]. G. Chen, T. Y. G. Tay, A. E. Davies, Y. Tanaka, and T. Takada, "Electrodes and Charge Injection in Low-density Polyethylene Using the Pulsed Electroacoustic Technique", IEEE Trans. Dielectr. Electr. Insul., vol. 8, no. 6, pp. 867–873, 2001.

[16]. H. Kon, Y. Suzuoki, T. Mizutani, M. Ieda, and N. Yoshifuji, "Packet-like space charges and conduction current in polyethylene cable insulation", IEEE Trans. Dielectr. Electr. Insul., vol. 3, no. 3, pp. 380–385, 1996.

[17]. D. Fabiani, G. C. Montanari, C. Laurent, G. Teyssedre, P. H. F. Morshuis, R. Bodega, L. a. Dissado, A. Campus, and U. H. Nilsson, "Polymeric HVDC cable design and space charge accumulation. Part 1: insulation/semicon interface", IEEE Electr. Insul. Mag., vol. 23, no. 6, pp. 11–19, 2007.

[18]. R. Patsch, "Space charge phenomena in polyethylene at high electric fields", J. Phys. D. Appl. Phys., vol. 23, no. 12, pp. 1497–1505, 2000.

[19]. Y. Zhang, J. Lewiner, C. Alquié, and N. Hampton, "Evidence of strong correlation between space-charge buildup and breakdown in cable insulation", IEEE Trans Dielectr. Electr. Insul., vol. 3, no. 6, pp. 778–783, 1996.

[20]. N. Hozumi, T. Takeda, H. Suzuki, and T. Okamoto, "Space Charge Behavior in XLPE Cable Insulation under 0 . 2-1 . 2 MV / cm dc Fields", IEEE Trans. Dielectr. Electr. Insul., vol. 5, no. 1, pp. 82–90, 1998.

[21]. *Power Cables with Extruded Insulation and their Accessories for Rated Voltages above 150 kV (U_m = 170 kV) up to 500 kV (U_m = 550 kV) Test Methods and Requirements*, IEC 62067, 2nd edition, 2011.

[22]. Recommendations for Testing DC Extruded Cable Systems for Power Transmission at a Rated Voltage Up To 500 kV, CIGRÉ Standard TB496, 2012.

[23]. C. K. Eoll, "Theory of Stress Distribution in Insulation of High-Voltage DC Cables: Part I," in *IEEE Transactions on Electrical Insulation*, vol. EI-10, no. 1, pp. 27-35, March 1975, doi: 10.1109/TEI.1975.297853.

[24]. C. C. Reddy and T. S. Ramu, "On the intrinsic thermal stability in HVDC cables," in *IEEE Transactions on Dielectrics and Electrical Insulation*, vol. 14, no. 6, pp. 1509-1515, December 2007, doi: 10.1109/TDEI.2007.4401235.

[25]. C. C. Reddy, "Theoretical Maximum Limits on Power-Handling Capacity of HVDC Cables," in *IEEE Transactions on Power Delivery*, vol. 24, no. 3, pp. 980-987, July 2009, doi: 10.1109/TPWRD.2009.2016624.

[26]. C. C. Reddy and T. S. Ramu, "On the computation of electric field and temperature distribution in HVDC cable insulation," in *IEEE Transactions on Dielectrics and Electrical Insulation*, vol. 13, no. 6, pp. 1236-1244, December 2006.

[27]. S. Whitehead, "*Dielectric Breakdown of Solids*," Oxford University Press, London, 1951.

[28]. L. Dissado and J. Fothergill, "Thermal breakdown," in *Electrical Degradation and Breakdown in Polymers*, ser. IET Materials and Devices Series. Peter Peregrinus, 1992.

[29]. Y. Liu, S. Zhang, X. Cao, C. Zhang and W. Li, "Simulation of electric field distribution in the XLPE insulation of a 320 kV DC cable under steady and time-varying states," in *IEEE Transactions on Dielectrics and Electrical Insulation*, vol. 25, no. 3, pp. 954-964, June 2018, doi: 10.1109/TDEI.2018.006973.

[30]. Y. O. Shaker, A. H. El-Hag, U. Patel and S. H. Jayaram, "Thermal modeling of medium voltage cable terminations under square pulses," in *IEEE Transactions on Dielectrics and Electrical Insulation*, vol. 21, no. 3, pp. 932-939, June 2014, doi: 10.1109/TDEI.2014.6832234.

[31]. N. Kovac, I. Sarajcev and D. Poljak, "Nonlinear-coupled electric-thermal modeling of underground cable systems," in *IEEE Transactions on Power Delivery*, vol. 21, no. 1, pp. 4-14, Jan. 2006, doi: 10.1109/TPWRD.2005.852272.

[32]. C. Garrido, A. F. Otero and J. Cidras, "Theoretical model to calculate steady-state and transient ampacity and temperature in buried cables," in *IEEE Transactions on Power Delivery*, vol. 18, no. 3, pp. 667-678, July 2003, doi: 10.1109/TPWRD.2002.801429.

[33]. T. L. Jones, "The calculation of cable parameters using combined thermal and electrical circuit models," in *IEEE Transactions on Power Delivery*, vol. 4, no. 3, pp. 1529-1540, July 1989, doi: 10.1109/61.32640.

[34]. G. J. Anders and M. A. El-Kady, "Transient ratings of buried power cables. I. Historical perspective and mathematical model," in *IEEE Transactions on Power Delivery*, vol. 7, no. 4, pp. 1724-1734, Oct. 1992, doi: 10.1109/61.156972.

[35]. X. Zhang and S. Pekarek, “A coupled thermal/electric circuit model for design of MVDC ship cables,” *2017 IEEE Electric Ship Technologies Symposium (ESTS)*, Arlington, VA, 2017, pp. 71-78, doi: 10.1109/ESTS.2017.8069262.

[36]. *Specification for Crosslinked Polyethylene Insulated PVC Sheathed Cables, part I,* Indian Standard IS:7098, 1988.

[37]. "IEEE Guide for Measuring Resistivity of Cable-Insulation Materials at High Direct Voltages," in *IEEE Std 402-1974 (Reaffirmed 1982)* , vol., no., pp.1-16, 8 Aug. 1974, doi: 10.1109/IEEESTD.1974.7409861.

[38]. Satoshi Nishikawa, Ken-Ichi Sasaki, Koji Akita, Masatoshi Sakamaki, Tatsuya Kazama And Kozo Suzuki, “XLPE Cable for DC Link,” in *Sei Technical Review*, April 2017, [Online] Available: https://global-sei.com/technology/tr/bn84/pdf/84-10.pdf.

[39]. S. Ogata *et al*., “Study on the dielectric characteristics of DC XLPE cables,” in *IEEE Transactions on Power Delivery*, vol. 5, no. 3, pp. 1239-1247, July 1990.

[40]. T. Takada, "Space Charge Formation in Dielectrics," in *IEEE Transactions on Electrical Insulation*, vol. EI-21, no. 6, pp. 873-879, Dec. 1986, doi: 10.1109/TEI.1986.348996.

[41]. X. Wang, N. Yoshimura, K. Murata, Y. Tanaka and T. Takada, "Space-Charge Characteristics in Polyethylene", *J. Appl. Phys.*, vol. 84, no. 3, pp. 1546-1550, 1998.

[42]. T. Mizutani, H. Semi and K. Kaneko, "Space charge behavior in low-density polyethylene," in *IEEE Transactions on Dielectrics and Electrical Insulation*, vol. 7, no. 4, pp. 503-508, Aug. 2000, doi: 10.1109/94.868069.

[43]. J. J. O’Dwyer, The Theory of Dielectric Breakdown of Solids, Oxford University Press, London, 1964.

[44]. X. Chen, C. Dai, L. Yu, C. Jiang, H. Zhou and Y. Tanaka, "Effect of thermal ageing on charge dynamics and material properties of 320 kV HVDC XLPE," in *IEEE Transactions on Dielectrics and Electrical Insulation*, vol. 26, no. 6, pp. 1797-1804, Dec. 2019, doi: 10.1109/TDEI.2019.008160.

[45]. J. S. Chahal and C. C. Reddy, "Dependence of space charge dynamics in LDPE on history of voltage application," in *IEEE Transactions on Dielectrics and Electrical Insulation*, vol. 23, no. 2, pp. 683-691, April 2016, doi: 10.1109/TDEI.2015.005317.

[46]. M. Fukuma, K. Fukunaga and T. Maeno, "Space charge dynamics in LDPE films immediately before breakdown," in *IEEE Transactions on Dielectrics and Electrical Insulation*, vol. 8, no. 2, pp. 304-306, April 2001, doi: 10.1109/94.919963.

[47]. K. Matsui *et al*., "Space charge behavior in low density polyethylene at pre-breakdown," in *IEEE Transactions on Dielectrics and Electrical Insulation*, vol. 12, no. 3, pp. 406-415, June 2005, doi: 10.1109/TDEI.2005.1453444.

[48]. Y. Tanaka, T. Kato, H. Suzuki, H. Miyake and T. Maeno, "Breakdown processes in low density polyethylene and cross-linked polyethylene under DC high stress," *Proceedings of 2014 International Symposium on Electrical Insulating Materials*, 2014, pp. 108-111, doi: 10.1109/ISEIM.2014.6870732.

[49]. C. C. Reddy and T. S. Ramu, "Polymer nanocomposites as insulation for HV DC cables - Investigations on the thermal breakdown," in *IEEE Transactions on Dielectrics and Electrical Insulation*, vol. 15, no. 1, pp. 221-227, February 2008, doi: 10.1109/T-DEI.2008.4446754.

[50]. K. Ishimoto *et al*., "Superiority of dielectric properties of LDPE/MgO nanocomposites over microcomposites," in *IEEE Transactions on Dielectrics and Electrical Insulation*, vol. 16, no. 6, pp. 1735-1742, December 2009, doi: 10.1109/TDEI.2009.5361597.

[51]. F. -B. Meng *et al*., "Effect of Thermal Ageing on Physico-Chemical and Electrical Properties of EHVDC XLPE Cable Insulation," in *IEEE Transactions on Dielectrics and Electrical Insulation*, vol. 28, no. 3, pp. 1012-1019, June 2021, doi: 10.1109/TDEI.2021.009449.

[52]. Zhichao Qiao,Wangsong Wu,Zhaowei Wang,Ling Zhang and Yuanxiang Zhou, “Space Charge Behavior of Thermally Aged Polyethylene Insulation of Track Cables”, *Polymers* **2022**, *14*(11), 2162; https://doi.org/10.3390/polym14112162 - 26 May 2022.

[53]. Y. Liu, H. Liu, L. Yu, Y. Li and L. Gao, "Effect of thermal stress on the space charge distribution of 160 kV HVDC cable insulation material," in *IEEE Transactions on Dielectrics and Electrical Insulation*, vol. 24, no. 3, pp. 1355-1364, June 2017, doi: 10.1109/TDEI.2017.006196.